Aire-Deficient C57BL/6 Mice Mimicking the Common Human 13-Base Pair Deletion Mutation Present with Only a Mild Autoimmune Phenotype[1]

François-Xavier Hubert,[2]* Sarah A. Kinkel,[†‡] Pauline E. Crewther,[†] Ping Z. F. Cannon,[†] Kylie E. Webster,[3†] Maire Link,[§] Raivo Uibo,[§] Moira K. O'Bryan,[¶] Anthony Meager,[‖] Simon P. Forehan,* Gordon K. Smyth,[††] Lauréane Mittaz,[4]** Stylianos E. Antonarakis,** Pärt Peterson,[‡‡] William R. Heath,[5]*[‡] and Hamish S. Scott[2,6†‡]

Autoimmune regulator (AIRE) is an important transcription regulator that mediates a role in central tolerance via promoting the "promiscuous" expression of tissue-specific Ags in the thymus. Although several mouse models of Aire deficiency have been described, none has analyzed the phenotype induced by a mutation that emulates the common 13-bp deletion in human APECED (autoimmune polyendocrinopathy-candidiasis-ectodermal dystrophy) by disrupting the first plant homeodomain in exon 8. Aire-deficient mice with a corresponding mutation showed some disturbance of the medullary epithelial compartment, but at the phenotypic level their T cell compartment appeared relatively normal in the thymus and periphery. An increase in the number of activated T cells was evident, and autoantibodies against several organs were detected. At the histological level, lymphocytic infiltration of several organs indicated the development of autoimmunity, although symptoms were mild and the quality of life for Aire-deficient mice appeared equivalent to wild-type littermates, with the exception of male infertility. Vβ and CDR3 length analysis suggested that each Aire-deficient mouse developed its own polyclonal autoimmune repertoire. Finally, given the prevalence of candidiasis in APECED patients, we examined the control of infection with *Candida albicans* in Aire-deficient mice. No increase in disease susceptibility was found for either oral or systemic infection. These observations support the view that additional genetic and/or environmental factors contribute substantially to the overt nature of autoimmunity associated with Aire mutations, even for mutations identical to those found in humans with APECED. *The Journal of Immunology,* 2009, 182: 3902–3918.

Autoimmune polyendocrinopathy-candidiasis-ectodermal dystrophy (APECED),[7] also known as autoimmune polyglandular syndrome type 1 (APS1), is an autosomal recessive disorder. APECED is an organ-specific human autoimmune disease that affects multiple organs, with both endocrine and nonendocrine tissues targeted for autoimmune destruction. The first symptoms that typically appear during early childhood include chronic mucocutaneous candidiasis, hypoparathyroidism, and primary adrenocortical failure. In adulthood, patients also develop endocrine autoimmune diseases, such as gonadal atrophy, type 1 diabetes, hypothyroidism, and hepatitis. Additionally, several ectodermic diseases, such as alopecia, nail dystrophies, and vitiligo, may arise (1). APECED is caused by mutations in the autoimmune

*Division of Immunology and [†]Division of Molecular Medicine, Walter and Eliza Hall Institute of Medical Research, Parkville, Victoria, Australia; [‡]Department of Medical Biology, University of Melbourne, Parkville, Victoria, Australia; [§]Immunology Group, Institute for General and Molecular Pathology, University of Tartu, Tartu, Estonia; [¶]Monash Institute of Reproduction and Development, Australian Research Council Centre of Excellence in Biotechnology and Development, Monash University, Clayton, Victoria, Australia; [‖]Biotherapeutics, National Institute for Biological Standards and Control, South Mimms, U.K.; **Department of Genetic Medicine and Development, University of Geneva Medical School, and University Hospitals, Geneva, Switzerland; [††]Division of Bioinformatics, Walter and Eliza Hall Institute of Medical Research, Parkville, Victoria, Australia; and [‡‡]Molecular Pathology, Biomedicum, Tartu University, Tartu, Estonia

Received for publication June 30, 2008. Accepted for publication January 2, 2009.

The costs of publication of this article were defrayed in part by the payment of page charges. This article must therefore be hereby marked *advertisement* in accordance with 18 U.S.C. Section 1734 solely to indicate this fact.

[1] This work was supported by fellowships from La Fondation pour la Recherche Medicale (FRM) and the Sixth Framework Programme of the European Union, Marie Curie, contract 040998 (to F.-X.H.), by Australian Postgraduate Awards (to S.A.K. and K.E.W.), the Swiss National Science Foundation (to S.E.A.), a Howard Hughes Medical Institute international scholar award (to W.R.H.), National Health and Medical Research Council (NHMRC) fellowships (171601 and 461204), NHMRC program grants (257501, 264573, 406700), Estonian targeted funding grant SF0180035s08 (to M.L. and R.U.), Euro-Thymaide and EurAPS, Sixth Framework Programme of the European Union, Wellcome Trust (to P.P.), and by the Nossal Leadership Award from the Walter and Eliza Hall Institute of Medical Research (to H.S.S.).

[2] Address correspondence and reprint requests to Dr. François-Xavier Hubert and Dr. Hamish Scott, Walter and Eliza Hall Institute of Medical Research, Melbourne, Victoria 3050, Australia. E-mail addresses: hubert@wehi.edu.au and hamish.scott@imvs.sa.gov.au

[3] Current address: Immunology and Inflammation, Garvan Institute of Medical Research, Darlinghurst, New South Wales, Australia.

[4] Current address: Division of Molecular Pediatrics, Maternité, Clinique Infantile 02-33, Centre Hospitalier Universitaire Vaudois, CH-1011 Lausanne, Switzerland.

[5] Current address: Department of Microbiology and Immunology, University of Melbourne, Parkville, Victoria 3010, Australia.

[6] Current address: Division of Molecular Pathology, Institute of Medical and Veterinary Science and The Hanson Institute, Box 14 Rundle Mall Post Office, Adelaide, South Australia 5000 and School of Medicine, University of Adelaide, Adelaide, South Australia 5005, Australia.

[7] Abbreviations used in this paper: APECED, autoimmune polyendocrinopathy-candidiasis-ectodermal dystrophy; AIRE, autoimmune regulator; APS1, autoimmune polyglandular syndrome type 1; β-gal, β-galactosidase; ES, embryonic stem; HSR, homogeneous staining region; LU, laboratory unit; mTEC, medullary thymic epithelial cells; MHC-II, MHC class II; PGK-Neo, phosphoglycerate kinase neomycin; PHD, plant homeodomain; SAND, Sp100, AIRE-1, NucP41/75, and DEAF-1; TEC, thymic epithelial cells; TSA, tissue-specific Ag; WT, wild type.

Copyright © 2009 by The American Association of Immunologists, Inc. 0022-1767/09/$2.00

www.jimmunol.org/cgi/doi/10.4049/jimmunol.0802124

regulator (AIRE) gene, which is encoded on chromosome 21q22.3 (2). AIRE is an important transcription factor mediating a role in central tolerance by promoting the "promiscuous" expression of tissue-specific Ags (TSA) in the thymus, which is associated with the negative selection of autoreactive T cells (3–6) and the generation of regulatory T cells (7).

While the literature concurs that Aire is expressed in medullary thymic epithelial cells (mTEC), it has also been reported that Aire is expressed in lymph nodes, in the peripheral monocyte/dendritic cell lineage (8–11), and, recently, in a subset of lymph node stromal cells (12, 13). However, the role of Aire expression in the periphery remains controversial (14).

At a molecular level, Aire contains several structural motifs common to nuclear proteins and transcription factors, including a nuclear localization signal (NLS), a putative homogeneous staining region (HSR) dimerization domain, a SAND domain (Sp100, AIRE-1, NucP41/75, and DEAF-1/suppressin), four LXXLL motifs, two plant homeodomain (PHD) zinc finger motifs, and a proline-rich region (2, 15). The first PHD zinc finger region of human AIRE has also been shown to function as an E3 ubiquitin ligase in vitro (16) and to bind to the N-terminal end of histone H3 (17). The importance of these domains for the function of Aire is highlighted by the mapping of most known human mutations to the HSR, recently characterized as a CARD (caspase recruitment domain) domain (18), and the PHD1 domain.

At present, three Aire-deficient mouse models have been reported. All of these models share a rather similar phenotype, which is considerably less severe than that of APECED patients (19–21). The first Aire-deficient mouse was generated to mimic the major mutation (p.R257X), found in the Finnish population, and the most common human APECED mutation, a termination codon in exon 6 (22). A second group generated Aire-deficient mice with an exon 2 deletion, which induces protein truncation just after the exon 1. This model was used to establish the role of Aire in expression of TSA, and both models have been used to demonstrate the important role of Aire in T cell education (3). Later, Kuroda et al. deleted a large proportion of the known functional domains of Aire, including SAND, PHD1, and PHD2 domains, to generate a third Aire-deficient mouse (19). All of these mice present with varying degrees of infertility, organ infiltration, circulating autoantibodies, activated T cells, and alteration of the repertoire of peripheral T cell. Studies using Aire-deficient mice on a C57BL/6 strain background have shown consistently that the phenotype of these mice is surprisingly mild. However, several groups have recently described that the strain used to generate Aire-deficient mice has a strong influence on the severity of the symptoms (20, 23). Recently, Su et al. presented a mechanism, using a novel murine model with a knockin G228W mutation in Aire, by which autoimmune predisposition to phenotypes distinct from APS1 can be mediated in a dominant-negative fashion by Aire (24).

None of the previously produced mouse models, however, has allowed analysis of an additional common APECED mutation in humans, namely the 13-bp deletion in human APECED (c.1094_1106del, p.L323fsX373) (25), which disrupts the PHD1 domain in exon 8, nor have these models examined susceptibility to infection with *Candida albicans*, normally the first and most common clinical symptom of APECED. Indeed, the c.1094–1106del mutation is the second most common in human APECED (26), and several analyses strongly suggest that this leads to expression of a stable truncated protein (27–29). Our results indicate that although a truncated protein is expressed and the medullary epithelial compartment is disturbed, the T cell compartment appears normal. There is, however, an increase in the number of activated T cells and detection of autoantibodies against several organs. At the histological level, lymphocytic infiltration of many different organs indicates the development of autoimmunity in $Aire^{-/-}$ mice. Despite the development of an autoimmune phenotype in these mice, it is mild and the quality of life appeared outwardly equivalent to wild-type (WT) littermates, with the exception of male infertility. $Aire^{-/-}$ mice were not hypersusceptible to infection with *C. albicans*.

Materials and Methods

Mice

All mice were C57BL/6 (B6) and bred and maintained at the Walter and Eliza Hall Institute for Medical Research. Aire knockout mice (C57BL6) were generated by a targeted disruption of the Aire gene. C57BL/6 mice were used at 6–10 wk of age unless indicated otherwise. All studies were performed according to protocols approved by the Melbourne Health Animal Ethics Committee.

Reagents

Abs were purchased from BD Pharmingen and were FITC-conjugated anti-Ly51 (clone 6C3) and anti-CD4 (clone L3T4); PE-conjugated anti-MHC class II (MHC-II) $I\text{-}A^{b,d,q}$ $I\text{-}E^{d,k}$ (clone M5/114.15.2), anti-CD25 (clone PC61.5), and anti-CD3 (clone 145-2C11); biotin-conjugated anti-Ly51 (clone 6C3), anti-CD69 (clone H1.2F3), and anti-CD44 (clone IM7); allophycocyanin-conjugated anti-CD45 (clone 30F11), anti-CD8 (clone 53-6.7), and anti-CD4 (clone L3T4); and streptavidin-PerCp5.5 used to reveal the biotin staining. Rat anti-Aire mAb was produced in the Monoclonal Antibody Facility at the Walter and Eliza Hall Institute of Medical Research (14). FITC anti-Vβ5 (clone MR9-4), Vβ8.1/8.2 (clone MR5-2), Vβ11 (clone RR3-15), and Vβ13 (clone MR12-3) Abs were purchased from BD Pharmingen, and biotin-conjugated anti-Vβ2, -Vβ3, -Vβ4, -Vβ6, -Vβ7, -Vβ9, -Vβ10, -Vβ12, and -Vβ14 were kindly provided by F. Carbone (Melbourne University, Melbourne, Australia).

Cell preparations

mTEC were enriched from the thymus as previously described (30). Briefly, thymi were collected into MT-RPMI and, following brief agitation using a wide bore glass pipette, the sample was subjected to enzymatic digestion. Thymic fragments were incubated in 5 ml of 0.125% (w/v) collagenase D with 0.1% (w/v) DNase I (Boehringer Mannheim) in MT-RPMI at 37°C for 15 min. Cells released into suspension were removed after the fragments had settled. This was repeated three to four times with fresh medium, and in the final digest the collagenase D was replaced with trypsin. Each cell suspension was counted and the final two or three enrichments were pooled. A negative depletion was performed to enrich for $CD45^-$ cells using CD45 microbeads (Miltenyi Biotec) and the autoMACS system (Miltenyi Biotec), as per the manufacturer's instructions. Cells were stained with Ly51-FITC (clone 6C3), MHC-II-PE (clone M5/114.15.2), and CD45-allophycocyanin (clone 30F11) mAbs, and $CD45^-MHC\text{-}II^{high}Ly51^{low}$ cells (mTEC) were sorted on a FACSAria instrument (BD Biosciences).

Flow cytometric analysis

The fluorescently-labeled preparations were analyzed on a FACSCalibur instrument (BD Biosciences). Color compensation was checked using appropriately stained cell controls. Four fluorescent channels were used for the immunofluorescence staining (FL1 for FITC, FL2 for PE, FL3 for PerCP5.5, and FL4 for allophycocyanin). mTEC preparations were labeled with anti-CD45 (clone 30F11), anti-MHC-II (clone M5/114.15.2), and anti-Ly51 (clone 6C3). The Aire intracellular staining was performed using the BD Cytofix/Cytoperm kit (BD Biosciences) according to the manufacturer's instructions.

TCR repertoire analysis

The immunoscope technique was used to evaluate TCR repertoire diversity by amplification of rearranged TCR Vβ-chain cDNAs (31). Each TCR Vβ family was assessed individually using forward TCR Vβ-specific primers and reverse constant β region (Cβ)-specific primers. The products were visualized by an elongation reaction using a nested fluorescent Cβ primer. The elongation products containing the CDR3 were separated by capillary electrophoresis (Applied Biosystems 3730 DNA analyzer). Size standard LIZ 500 (Applied Biosystems) was applied to each run. The PCR product was denatured by addition of formamide and heat to produce single-stranded products. The results were analyzed using GeneMapper software

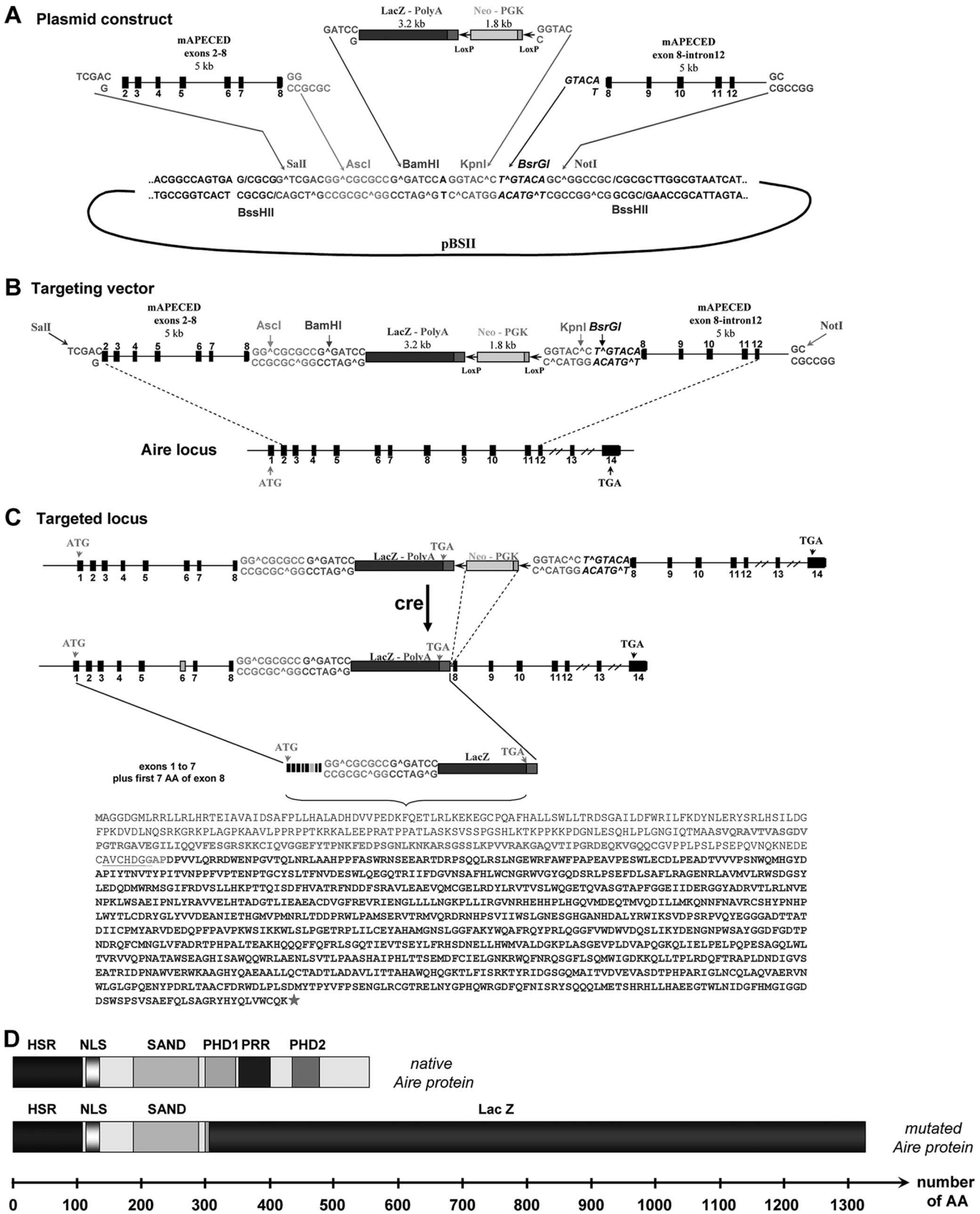

FIGURE 1. The Aire gene knockout construct. *A*, Plasmid construct used for the generation of Aire knockout mice. *B*, The Aire gene was disrupted by homologous recombination with the targeting vector in C57BL/6 ES cells. *C*, The PGK-Neo cassette was used to select positive recombination events and was later removed using the flanking LoxP sites and Cre recombinase. This recombination event places the LacZ reporter gene under the control of the endogenous Aire promoter in fusion with exon 8, disrupting exon 8 and thus the first PHD finger domain. Three stop codons and a polyadenylation signal (PolyA) were included to prevent any transcription of full-length Aire. This encodes a truncated Aire protein size of 1328 aa containing the first 310 aa of native Aire. Restriction endonuclease sites: BG, BsrG1; M, Mlu1; S, *Sal*I. *D*, Schematic representation of normal Aire protein (*top*) and truncated Aire fusion protein (*bottom*).

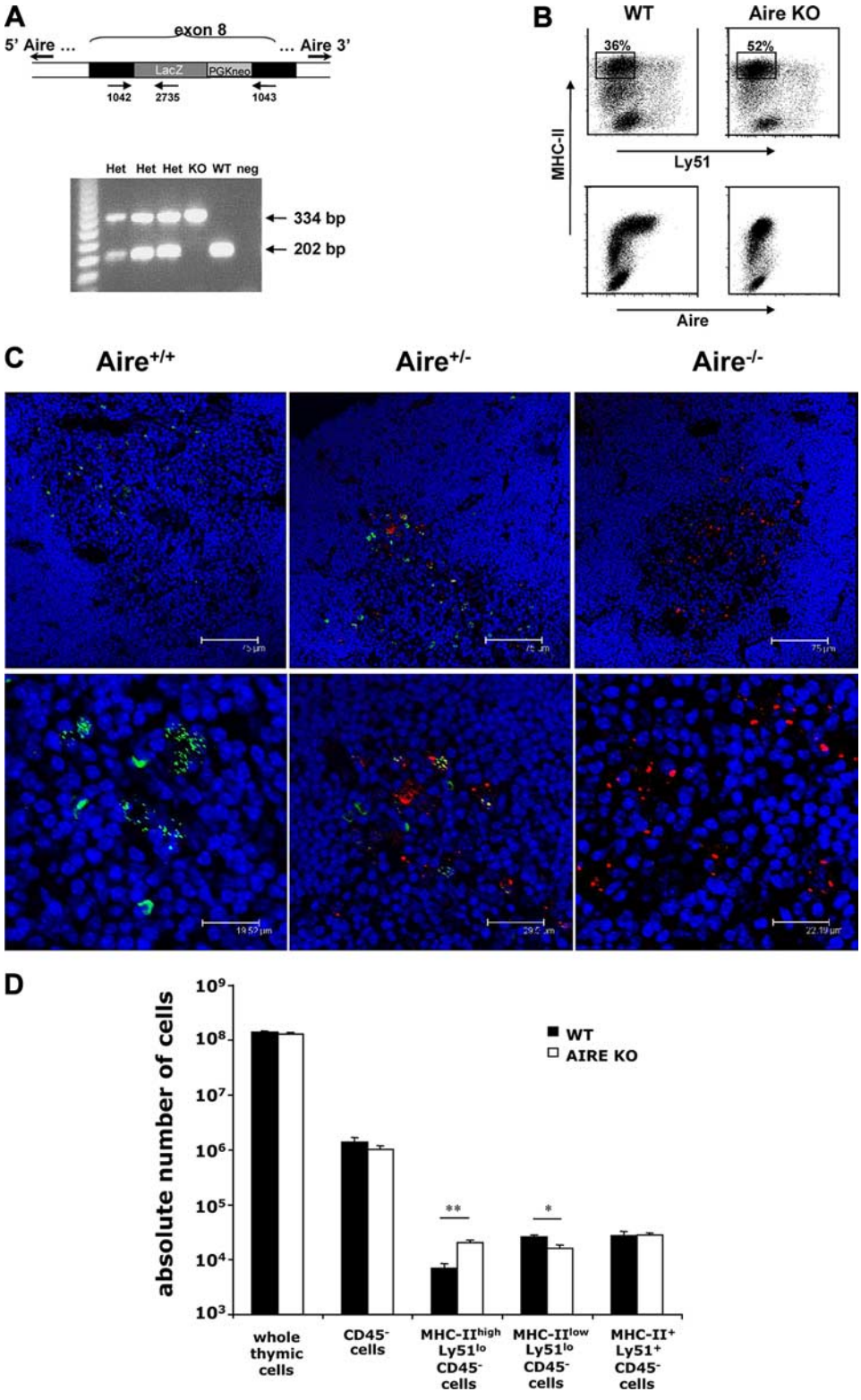

FIGURE 2. Analysis of Aire expression and the thymic compartment of Aire$^{-/-}$ mice. *A*, Four- to 6-wk-old C57BL/6 mice were genotyped by PCR from tail genomic DNA. *B*, Aire is expressed by specific nonhematopoietic thymic cells: CD45^{-}MHC-II^{high}Ly51^{low}. A negative depletion was performed to enrich for CD45^{-} cells and analyzed for their expression of CD45, MHC-II, Ly51, and Aire. After gating on CD45^{-} cells, mTEC (boxed areas) are distinguished from other cell subsets according to their expression of MHC-II and Ly51 (*top row*). Aire expression is compared with MHC-II expression on CD45^{-} cells. *C*, Aire immunofluorescence on thymic sections. Tissues from WT, Aire heterozygous, and Aire-deficient mice were stained with an anti-Aire Ab (green), anti-β-gal Ab (red), and Hoechst (blue). The immunofluorescence was visualized by laser scanning confocal microscopy. Each row represents different magnifications with scales indicated. *D*, Estimation of the number of CD45^{-} cells and CD45^{-}MHC-II^{high}Ly51^{low} cells in single 6-wk-old thymus: each single thymus was digested and stained for analysis of expression of CD45, MHC-II, and Ly51. Sample data from 2×10^4 CD45^{-} cells were acquired and results are expressed on a logarithmic *y*-axis as mean $\pm$ SD of eight mice per group.

version 3.7 (Applied Biosystems) and are shown as graphic distribution of size peaks centered on a peak corresponding to a CDR3 of 8–10 amino acids. Normal profiles have a Gaussian-like distribution of an average of six to eight peaks per TCR Vβ family (polyclonal Gaussian). The peaks are spaced by three nucleotides. Comparisons with size standards from WT mice showed that they corresponded to in-frame transcripts. Alterations in the normal profile result in a polyclonal skewed profile, causing a shift in the center of the CDR3 distributions or a disruption of the normal peak distribution due to clonal T cell expansions. Data are expressed as percentage of oligoclonal, polyclonal skewed, or polyclonal Gaussian Vβ families per total number of Vβ families amplified from a sample. A unique length of the CDR3 is not necessarily associated with the same sequence, and the number of transcripts with a given length of CDR3 is proportional to the area under the peak. Then, for each CDR3 length profile experiment, the normalized profile was compared with the sample one, and the difference was plotted on a graph, according to the CDR3 length and percentage of perturbation. This first analysis step only gives qualitative information, because there is no indication of the amount of Vβ altered. Percentages of CDR3-length distribution alterations are represented as a color code, from deep green to dark red. The *x*-axis displays the mouse Vβ families; the *y*-axis gives the CDR3 lengths.

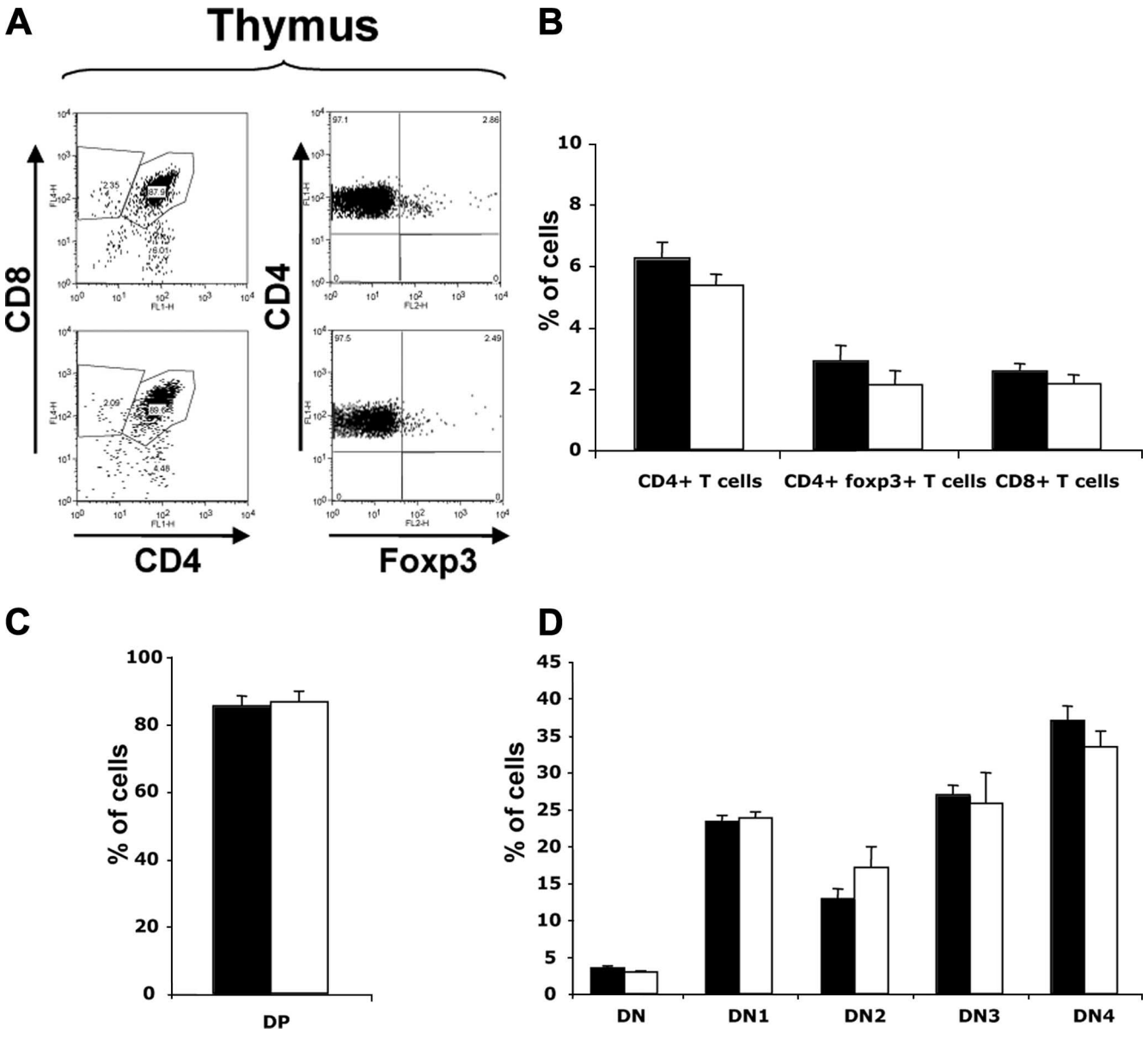

FIGURE 3. Thymic T cell compartment in Aire-deficient mice (open bars) vs WT mice (filled bars). Each thymus was crushed through a sieve and the cells were stained with CD4-FITC, Foxp3-PE, and CD8-allophycocyanin and acquired on a FACSCalibur. Four subsets were distinguished: $CD4^+CD8^-$ T cells, $CD4^-CD8^+$ T cells (*A* and *B*), double-positive $CD4^+CD8^+$ thymocytes (DP) (*A* and *C*), and double-negative $CD4^-CD8^-$ thymocytes (DN) (*A* and *D*). Foxp3 expression was analyzed on $CD4^+CD8^-$ T cells (*A* and *B*). The same cells were stained with CD4-FITC, CD25-PE, CD44-biotin, and CD8-allophycocyanin. After gating on $CD4^-CD8^-$ cells, four double-negative thymocyte subsets were distinguished according the expression of CD25 and CD44: DN1 ($CD44^+CD25^-$), DN2 ($CD44^+CD25^+$), DN3 ($CD44^-CD25^+$), and DN4 ($CD44^-CD25^-$) (*D*); *y*-axis as mean ± SD of six mice.

Western blot analysis

After homogenization on ice, testis, liver, lung, salivary gland, pancreas, and eye tissue from $Rag^{-/-}$ mice were lysed and boiled in a buffer containing 1% SDS, 10% glycerol, 10% 2-ME, 40 mM Tris (pH 6.8), and 0.01% bromophenol blue. Equal amounts of cell lysate were run on a 12% Tris-glycine polyacrylamide gel (Invitrogen) and then transferred to a Hybond-ECL Western membrane (Amersham) at 50 V for 40 min. The membrane was blocked for 4 h in a 5% milk solution in PBS and was incubated overnight at 4°C with sera from Aire-deficient or WT mice diluted 1/500. The membrane was washed several times with PBS and 0.1% Tween 20 and then incubated with secondary Ab, HRP-conjugated sheep anti-mouse IgG (1/1000; Amersham), for 1 h. Detection of staining was performed using ECL Western blotting detection reagents (Amersham) according to the manufacturer's instructions.

Radioimmunoassays

Abs to insulin were detected as described in Yu et al. (32) with slight modifications. Briefly, ^{125}I-insulin (Amersham) (~20,000 cpm) was incubated with 3 μl of serum with or without unlabeled human insulin at 1/5 dilution of serum for 3 days at 4°C in buffer A (20 mM Tris-HCl buffer (pH 7.4) containing 150 mM NaCl, 1% BSA, 0.15% Tween 20, and 0.1% sodium azide) on a end-over-end shaker. Fifty microliters containing 50% protein A-Sepharose and 8% protein G-Sepharose (Amersham) was added and incubated for 45 min at 4°C on an end-over-end shaker. The samples were washed four times with 1 ml of cold buffer B (20 mM Tris-HCl buffer (pH 7.4) containing 150 mM NaCl, 0.15% Tween 20, and 0.1% sodium azide) and transferred to scintillation tubes with 3× 100 μl of buffer B.

Mouse Cyp1a2 and Gad65 cDNAs were amplified with primers mCYP-F1 (ATGGCGTTCTCCCAGTACATCT) and mCYP-R1 (TCACT TGGAAAAGCGTGGC) and mGAD-F1 (ATGGCGTCTCCTGGCTCC) and mGAD-R1 (TTACAAATCTTGTCCGAGGCG), respectively. The full-length cDNAs were cloned into pCR2.1-TOPO vector using a TOPO TA cloning kit (Invitrogen). The plasmids containing Cyp1a2 and Gad65 cDNAs were in vitro transcribed and translated using a TNT-coupled transcription and translation kit (Promega) using [^{35}S]methionine. In vitro translated mouse Gad65 and Cyp1a2 were purified through the Sephadex G-25 DNA grade column. The Ags (~40,000 cpm) were suspended in 50

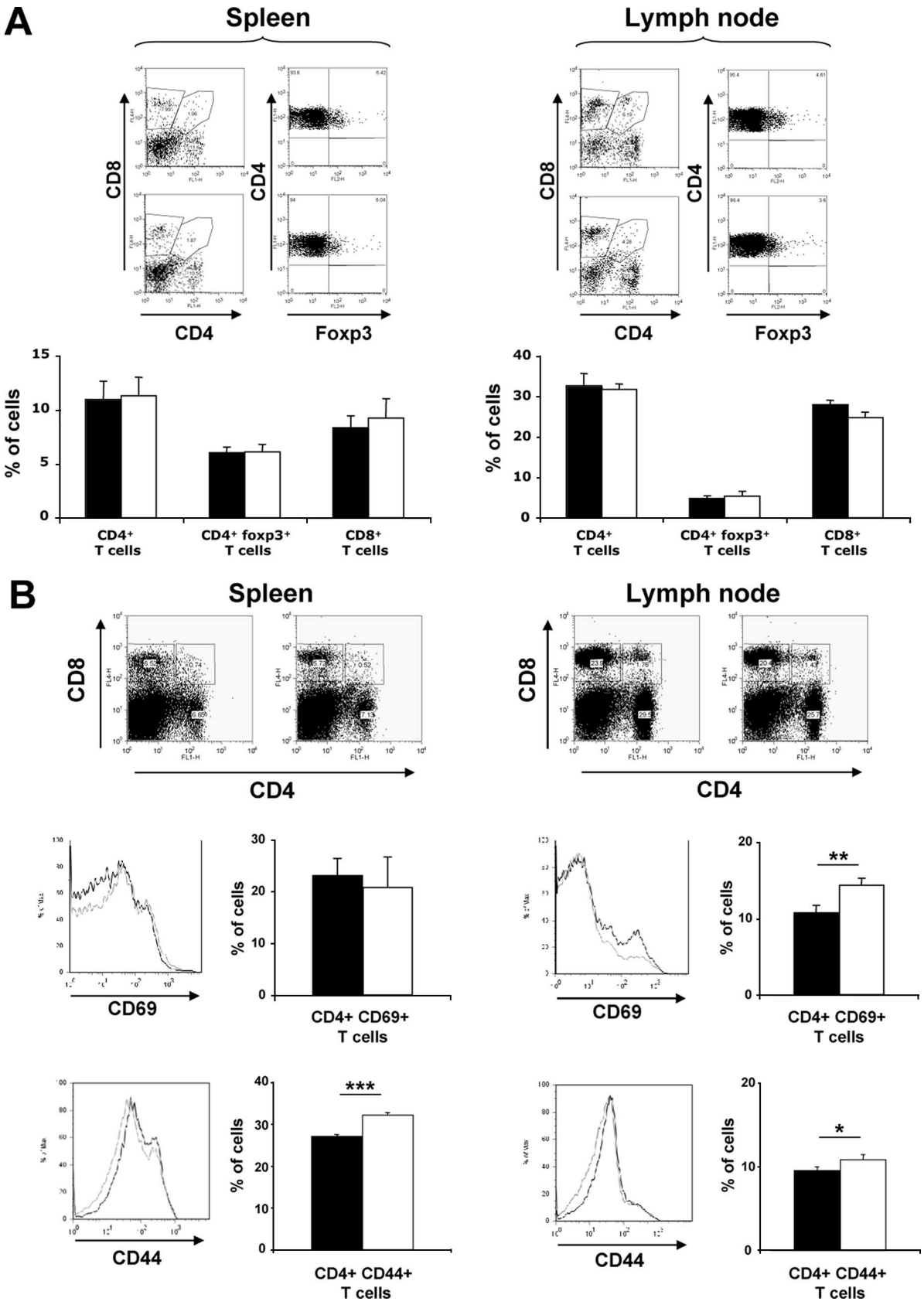

FIGURE 4. Peripheral T cell compartment in Aire-deficient mice vs WT mice. *A*, Spleen or lymph node organs were crushed through a sieve and the cells were stained with CD4-FITC, Foxp3-PE, and CD8-allophycocyanin and acquired on a FACSCalibur. Two subsets were distinguished: $CD4^+CD8^-$ T cells and $CD4^-CD8^+$ T cells. Foxp3 expression was analyzed on $CD4^+CD8^-$ T cells; *y*-axis as mean ± SD of six mice. *B*, Activated $CD4^+$ T cells in periphery in Aire-deficient mice (open bars) vs WT mice (filled bars) were analyzed according to CD69 or CD44 expression. Cells were then stained with CD4-FITC, CD8-allophycocyanin, and CD69-biotin or CD44-biotin and acquired on a FACSCalibur. The proportion of early activated $CD69^+CD4^+$ T cells or of activated/memory $CD44^+CD4^+$ T cells is estimated in a bulk of $CD4^+CD8^-$ T cells; *y*-axis as mean ± SD of six mice.

μl of RIP buffer (150 mM NaCl, 10 mM Tris-HCl (pH 7.4), 0,005% Tween 20, aprotinine 1/1000, leupeptine 1/1000), and 50 μl of 1/10 diluted mouse serum was added and incubated for 30 min at room temperature. Subsequently, 10 μl of protein G-Sepharose (Amersham Biosciences) was added and incubated for 1 h at room temperature. The samples were washed four times with RIP buffer. Abs to *C. albicans* enolase and Hsp90 were detected by radioimmunoassay using in vitro translated/transcribed proteins as described earlier.

In all radioimmunoassays, 3 ml of liquid scintillation cocktail (Optiphase HiSafe3; PerkinElmer) was added for signal detection and counted in a scintillation counter. The results are expressed as absolute values. The value of positive control for insulin (a human serum from a person with type 1 diabetes) was ~4000 cpm.

Antiviral IFN neutralization assays

For detection of mouse IFN-αA (Mu-IFN-αA; PBL Laboratories), mouse L-929 cells (American Type Culture Collection CCL-1) were pretreated with dilute Mu-IFN-αA (10 laboratory units (LU)/ml) that had been preincubated for 2 h with serial dilutions of test sera or neutralizing rat anti-Mu-IFN-α mAb (PBL Laboratories). Following incubation at 37°C for 24 h, the cells were challenged with encephalomyocarditis virus for 24 h, stained with 0.05% amido blue-black, fixed with 4% formaldehyde in acetic acid buffer, and stain-eluted with 0.15 ml of 0.05 M sodium hydroxide before absorbances were read at 620 nm. The neutralizing Ab titer was the reciprocal of the dilution of serum that reduces 10 LU/ml Mu-IFN-αA to 1 LU/ml (the normal endpoint of antiviral assays) (33, 34). The cutoff for positivity was a titer of 40.

Expression analysis

RNA extraction from WT and Aire-deficient mTEC was performed using the RNeasy Micro kit (Qiagen) according to the manufacturer's instructions. RNA amplification was done at the Australian Genome Research Facility, following the Affymetrix manual (701725 rev5). Briefly, 100 ng of total RNA was amplified using T7-oligo(dT) and the MEGAscript T7 kit (Ambion). A second round of cDNA synthesis was performed using first round-amplified RNA. Amplified RNA was biotin-labeled using the GeneChip IVT labeling kit. Fifteen micrograms of labeled RNA was then fragmented as described in the Affymetrix manual. The Mouse Genome 430 2.0 arrays were hybridized overnight, washed, and scanned using a GeneChip scanner 3000 (Affymetrix). For analysis of the Affymetrix GeneChips, the intensities for each probe set were normalized and summarized using the robust multiarray analysis algorithm (35). Analysis of the microarray and PCR expression data was undertaken using the limma software package of the Bioconductor Project (36). Differential expression between WT and Aire-deficient samples was assessed using linear modeling and empirical Bayes moderated *t* statistics (37). Values of *p* were adjusted using the Benjamini and Hochberg method to control the false discovery rate at 0.05. The microarray experiment contained three WT samples, two Aire-deficient samples, and three other closely related sample,s which were included in the linear model but not used to compute the *t* statistics. Array data were deposited into the Gene Expression Omnibus public database (www.ncbi.nlm.nih.gov/geo/query/acc.cgi?acc, accession no. GSE14365).

Reverse transcription was performed using SuperScript III RNase H-reverse transcriptase (Invitrogen), with 250 ng of random primers (Promega) per reaction according to the manufacturer's instructions. Quantitative real-time PCR was performed on the ABI Prism 7900HT sequence detection system using prevalidated TaqMan assays and TaqMan Universal Master Mix with AmpliTaq Gold (Applied Biosystems) as per the manufacturer's instructions. *Ct* values were determined using ABI Prism SDS version 2.2 (Applied Biosystems), and relative expression was calculated using the $2^{-\Delta\Delta Ct}$ method. The PCR experiment contained two WT and two Aire-deficient samples. In this case, moderated paired *t* statistics were used to account for any differences between two processing times.

Infertility test

Sperm collected from mice was incubated for 2 h in mT6 before in vitro fertilization. Oocytes were collected from (CD57BL/6 $\times$ CBA)F_1 mice and incubated for 6 h with sperm from the above mice. Fertilization and different stages of embryo development (two cells, four cells, morulae, and blastocyst) were enumerated (38).

Histology

Dissected tissues were immersed in Bouin's fixative overnight and then washed with 70% ethanol. Fixed tissues were then embedded in paraffin using standard method and then sectioned, at 2-μm thickness, onto glass slides and stained with H&E.

Organ infiltration

The organs from 5-mo-old mice were digested three times at 37°C in fresh medium containing 1 mg/ml collagenase D and 2 μg/ml DNaseI (Roche). Cells were filtered through a 100-μm mesh to remove clumps, and samples were treated with 0.15 M NH_4Cl for lysis of erythrocytes. Cell preparations were labeled with anti-CD4, anti-CD8, and anti-CD3 and either anti-CD69 or anti-CD44.

Immunofluorescence

Acetone-fixed 5-μm thymus sections from WT, $Aire^{+/-}$, and $Aire^{-/-}$ mice were stained with rat anti-Aire-FITC (clone 5H12) and rabbit anti-β-galactosidase (β-gal; a kind gift from E. Handman, Walter and Eliza Hall Institute, Melbourne) with Alexa Fluor 546 donkey anti-rabbit IgG (Invitrogen). After washing, sections were stained with Hoechst 33342 (Sigma-Aldrich) for 5 min and washed a further three times. Sections were mounted and cover-slipped using fluorescent mounting medium (Dako) before viewing with confocal or fluorescent microscopy.

Yeast infection

C. albicans isolate 3630 was obtained from the Mycology Reference Laboratory at the Royal North Shore Hospital, Sydney, Australia (a kind gift from Dr. R. B. Ashman) and stored at −70°C in Sabouraud's broth/15% (v/v) glycerol. Strain 3630 was isolated from the nail of a patient with cutaneous candidiasis. For use, yeasts were grown in Sabouraud's broth for 48 h at room temperature with continuous agitation on a magnetic stirrer. Blastospores were washed in PBS and adjusted to the appropriate concentration for inoculation. For oral infection, mice were inoculated orally with 10^8 live *C. albicans* in 20 μl of sterile PBS. The infection was monitored by swabbing the oral cavity on days 1, 4, 8, 14, 18, and 21, with sterile cotton swabs moistened with sterile PBS, and directly plating on Sabouraud's agar plates. Agar plates were incubated for 48 h at 30°C. All inoculation and sampling procedures were conducted under anesthesia. CFU were counted on Sabouraud's agar plates and the counts were assigned into five groups correlating with the level of recoverable yeast from the oral cavity, as previously described (39). This provided a semiquantitative measure of the level of floridity of the infection. The scoring system used was as follows: 0, no detectable yeast; 1, 1–10 CFU/plate; 2, 11–100 CFU/plate; 3, 101-1000 CFU/plate; 4, ≥1001 CFU/plate. For systemic infection, mice were injected with 3×10^5 *C. albicans* 3630 in 200 μl of PBS via the tail vein. Mice were sacrificed on day 5 after infection. The kidneys were harvested, weighed, suspended in 1 ml of sterile PBS, and homogenized. Then, 100 μl of suspension was titrated in duplicate on Sabouraud's agar plates, incubated at 30°C for 48 h, and colonies were counted. The results were expressed as $\log_{10}$ CFU/g tissue.

Results

Disruption of the Aire gene in exon 8

To investigate the biological functions of Aire, we generated mice deficient for this gene via homologous recombination of targeting vectors in mouse embryonic stem cells (Fig. 1). Insertion of the Aire targeting vector disrupted exon 8 and brought the LacZ reporter gene under the control of the endogenous Aire promoter, creating an Aire-LacZ fusion gene. A phosphoglycerate kinase neomycin (PGK-Neo) cassette was used to select positive recombination events and was later removed using the flanking LoxP sites and Cre recombinase (Fig. 1, *A* and *B*). This insertion was designed to interrupt the PHD1 domain, reflecting the common 13-bp deletion in human APECED patients, localized after the SAND domain and within the PHD1 domain (c.1094_1106del, p.L323fsX373) (25). Three stop codons and a polyadenylation signal were also included to prevent any transcription of full-length Aire (Fig. 1*C*). We verified the targeted disruption by three-primer PCR, showing a band at 202 bp for the WT locus and a band at 334 bp for the knockout locus (Fig. 2*A*). As previously described (14), Aire protein expression was not detected by flow cytometry, confirming Aire deficiency (Fig. 2*B*). Examination of $CD45^-$ cells from WT mice for expression of MHC-II and Aire showed that

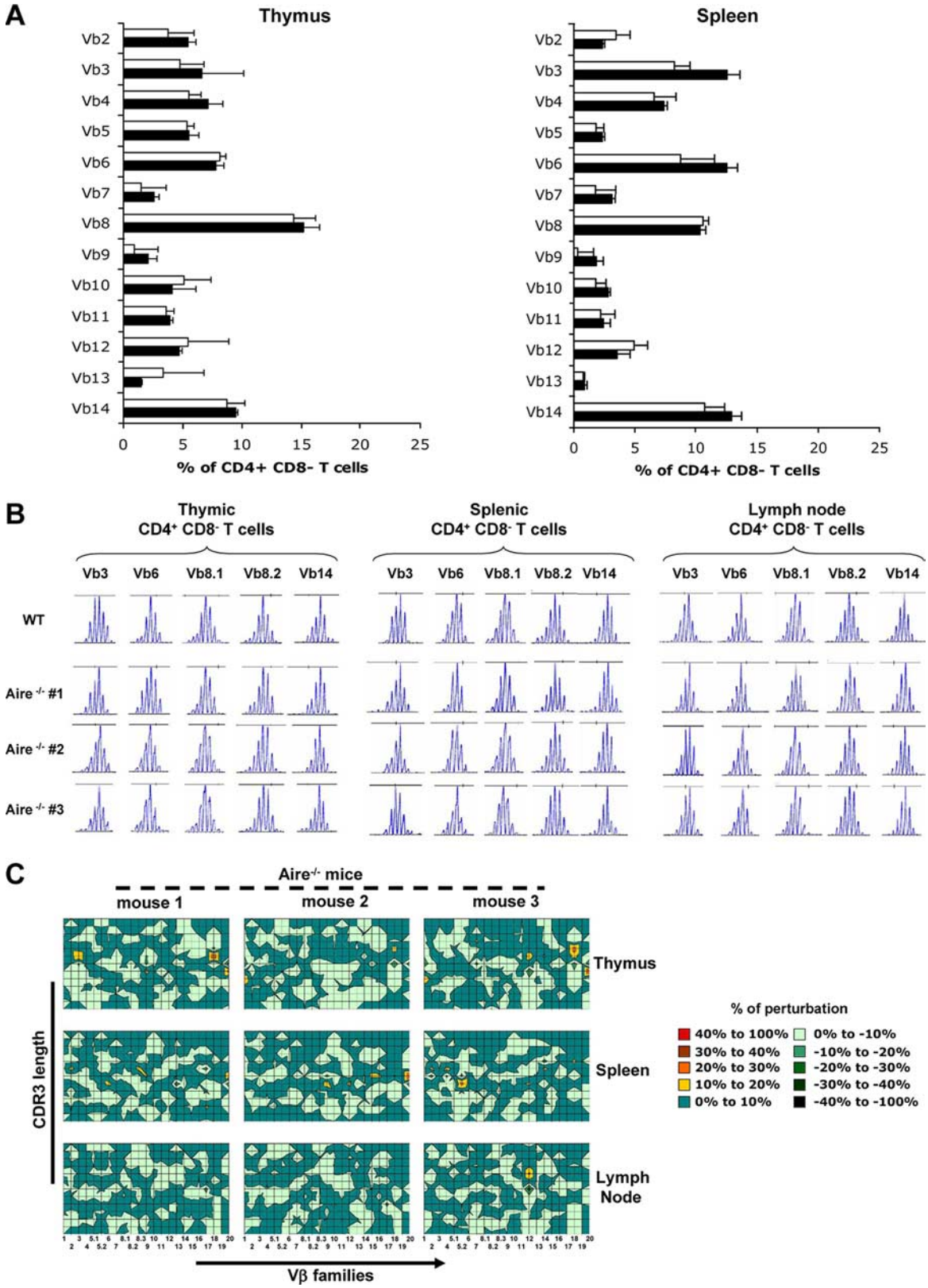

FIGURE 5. Vβ repertoire of CD4$^+$ T cell from Aire-deficient and WT mice. *A*, Vβ repertoire of CD4$^+$ T cell from Aire-deficient mice (open bars) vs WT mice (filled bars). Thymus or spleen organs were crushed through a sieve and cells were then stained to CD4, CD8, CD25, and different Vβ and acquired on a FACSCalibur. The proportion of different Vβ^+CD4$^+$ T cells is estimated in a bulk of CD4$^+$CD8$^-$ T cells; *y*-axis as mean $\pm$ SD of six mice. *B*, Variations in both length and distribution of the most variable region of the TCR Vβ-chain, the CDR3, using the immunoscope method. Examples of immunoscope of major Vβ families from CD4$^+$ T cells according to their different CDR3 lengths in thymus, spleen, and lymph node are shown. The alteration was determined by comparing the immunoscope profile of each population of CD4$^+$ T cells from WT mice to CD4$^+$ T cells from each Aire-deficient mouse. *C*, Views representing the percentage of perturbation in each different CDR3 length found in each Vβ family. Comparisons with size standards from WT mice show that they correspond to in-frame transcripts. Alterations of the normal profile result in a polyclonal skewed profile, leading to a shift in the center of CDR3 distribution or a disruption of the normal peak distribution due to clonal T cell expansions (see *Materials and Methods*).

only MHC-II^{high} cells expressed Aire (14). Interestingly, we observed a greater proportion of these cells in Aire-deficient mice compared with WT mice (Fig. 2*B*). While these findings demonstrate that native Aire is absent in Aire-deficient mice, they did not exclude the expression of a truncated Aire protein. Insertion of a LacZ reporter into the *Aire* gene generates an Aire-β-gal fusion protein. Staining with an anti-β-gal Ab revealed β-gal expression in Aire$^{+/-}$ and Aire$^{-/-}$ thymi (Fig. 2*C*), as previously reported (14). Interestingly, β-gal colocalized with native Aire as shown in Fig. 2*C* in Aire$^{+/-}$ thymi, suggesting an ability of the fusion protein to correctly localize to nuclear bodies and perhaps to dimerize. However, in the thymi of our Aire-deficient mice, β-gal was expressed within the nucleus to a lesser extent than seen in the heterozygote and did not show the typical speckled staining pattern of Aire, but rather appeared to form several larger speckles that may have be an aggregation of nonfunctional fusion protein.

Thymic epithelial cell compartment is disturbed

It has been established that cortical and medullary epithelial cells can be distinguished from cells of hematopoietic origin by their lack of expression of CD45 and can be identified according to the expression of MHC-II and Ly51, with both populations expressing high levels of MHC-II but only cortical thymic epithelial cells (cTEC) expressing Ly51 (14). Thus, after the elimination of contaminant CD45$^+$ cells, four major populations of CD45$^-$ cells were distinguished: MHC-II^{high}Ly51^{low} (mature mTEC), MHC-II^{low}Ly51^{low} (progenitor or immature mTEC), MHC-II$^-$Ly51^{low} (fibroblast and endothelial cells), and MHC-II^{high}Ly51$^+$ (cTEC). Because the enrichment procedure used above for preparing CD45$^-$ cells may have affected the proportion of different subpopulations of TECs, we decided to examine the phenotype of these subpopulations within nonenriched thymus populations, after simple enzymatic digestion and red cell elimination. Despite TEC populations being very rare, it was still feasible to enumerate CD45$^-$ cells and their subpopulations in WT and Aire$^{-/-}$ mice (Fig. 2*D*). Based on these analyses, we estimated that CD45$^-$ cells represented 1 $\pm$ 0.4% and 0.8 $\pm$ 0.2% of a whole thymus in WT and Aire$^{-/-}$ mice, respectively. Of CD45$^-$ cells, the MHC-II^{high}Ly51^{low} subset made up 0.5 $\pm$ 0.2% in WT and 2.1 $\pm$ 0.3% in Aire$^{-/-}$ mice (Fig. 2*D*). Thus, Aire$^{-/-}$ mice had ~4-fold more MHC-II^{high} mTEC than did WT littermates. Complementary to this, the immature mTEC (imTEC) compartment, considered to be CD45$^-$MHC-II^{low}Ly51^{low}, was reduced by 25% in the Aire$^{-/-}$ mice. Thus, the mTEC/imTEC ratio was 0.3 $\pm$ 0.16 and 1.3 $\pm$ 0.3 in WT and Aire$^{-/-}$ mice, respectively. The cortical compartment remained consistent between WT and Aire$^{-/-}$ mice, representing 2.5 $\pm$ 0.8% of CD45$^-$ cells, with the total epithelial cell compartment representing only ~5% of the CD45$^-$ thymic stromal cell population. In summary, although the architecture of the thymus appeared to be largely normal and unmodified (14), as reported in other Aire-deficient models, the epithelial compartment appeared to be biased toward mature mTEC in Aire$^{-/-}$ mice. These data establish that the impact of Aire deficiency extends beyond the lack of expression of a subset of TSA in mature mTEC and affects changes in the thymic environment that would be compatible with a role for Aire in mTEC differentiation and/or survival.

Central T cell compartments appear normal

Aire is an important mediator of central tolerance that promotes the promiscuous expression of TSA in the thymus (40), shown to be associated with the negative selection of autoreactive T cells (4, 6). Recently, Aire has also been reported to have a role in the generation of regulatory T cells within the thymus (7). Furthermore, our demonstration that the ratio of mature-to-immature mTEC is altered suggests other potential effects on T cell education. Given these results, we decided to examine the T cell compartment in different immunological organs (thymus, spleen, and lymph node). After staining thymocytes for CD4, CD8, and Foxp3, we discriminated CD4$^+$ and CD8$^+$ single-positive and double-positive T cells and identified regulatory CD4$^+$ T cells by their expression of Foxp3 (Fig. 3). No significant difference was observed for any of these populations, although a trend toward a decreased proportion of CD4$^+$, CD8$^+$, and CD4$^+$ Foxp3$^+$ T cells was noted. Moreover, the level of Foxp3 staining was slightly, although not significantly, reduced in Aire$^{-/-}$ mice (Fig. 3*A*). When the double-negative (CD4$^-$CD8$^-$) compartment was analyzed for expression of CD44 and CD25, no significant difference was observed, demonstrating minimal impact of Aire on early thymocyte development (Fig. 3*D*). Taken together, these results show that in terms of proportion and number, the T cell compartment is not significantly modified, suggesting a minimal impact of Aire on thymocyte maturation, as has been previously reported by others (41). However, this does not exclude a significant role for Aire in the fate of certain TSA-specific cells. Indeed, Aire was previously found to be necessary for normal clonal deletion in OT-II/RIP-mOVA double-transgenic animals as well as in other TCR neo-self-Ag double-transgenic systems (6). Using the same system, our Aire-deficient mice show a severe defect in their ability to delete CD4$^+$ autoreactive thymocytes (F. X. Hubert, H. S. Scott, W. R. Heath, unpublished data).

Increased number of peripheral activated T cells in Aire$^{-/-}$ mice

Although the mTEC compartment was perturbed and there was a defect in the negative selection process in the thymus of our Aire$^{-/-}$ mice, an analysis of peripheral lymphoid organs revealed no obvious differences in the number or proportion of CD4$^+$ T cells, CD4$^+$ Foxp3$^+$ T cells, or CD8$^+$ T cells in the spleen and lymph node of Aire$^{-/-}$ mice compared with WT mice (Fig. 4*A*). As Aire is involved in T cell selection and plays an important role in preventing autoimmunity (3, 4, 6), we analyzed whether Aire$^{-/-}$ mice may have a greater proportion of activated T cells (Fig. 4*B*), potentially reflecting the presence of autoimmunity. Examination of CD69 expression on CD4$^+$ T cells as an early activation marker showed no difference in the spleen (23 $\pm$ 3% in WT mice, 20 $\pm$ 5% in Aire$^{-/-}$ mice), but a 5% increase was observed in lymph nodes of Aire$^{-/-}$ mice (10 $\pm$ 0.6% in WT mice, 15 $\pm$ 0.5% in Aire$^{-/-}$ mice). Analysis of the proportion of CD44^{high}CD4$^+$ T cells (Ag-experienced cells) in the same organs (Fig. 4*B*) revealed a significant increase in these cells in the spleen (27 $\pm$ 0.8% in WT mice, 32 $\pm$ 1.2% in Aire$^{-/-}$ mice) and lymph node (9 $\pm$ 0.3% in WT mice, 11 $\pm$ 0.4% in Aire$^{-/-}$ mice) of Aire$^{-/-}$ mice. Interestingly, examination of the same activation markers on CD8$^+$ T cells did not reveal any significant differences (data not shown).

Vβ repertoire of CD4$^+$ T cells

The modest increase of activated CD4$^+$ T cells in Aire$^{-/-}$ mice could be the result of an overrepresentation of T cells that are normally destined for negative selection. To examine whether this possibility is reflected by an alteration in the Vβ repertoire, we analyzed TCR Vβ expression on thymic and splenic CD4$^+$ T cells using flow cytometry (Fig. 5*A*). While the Vβ repertoire differed somewhat between thymic and peripheral CD4 T cells, no difference was observed between WT and Aire$^{-/-}$ mice. This indicated that there was no overt difference in Vβ selection in mutant mice. The same observations were made for thymic and splenic CD8$^+$ T cells (data not shown).

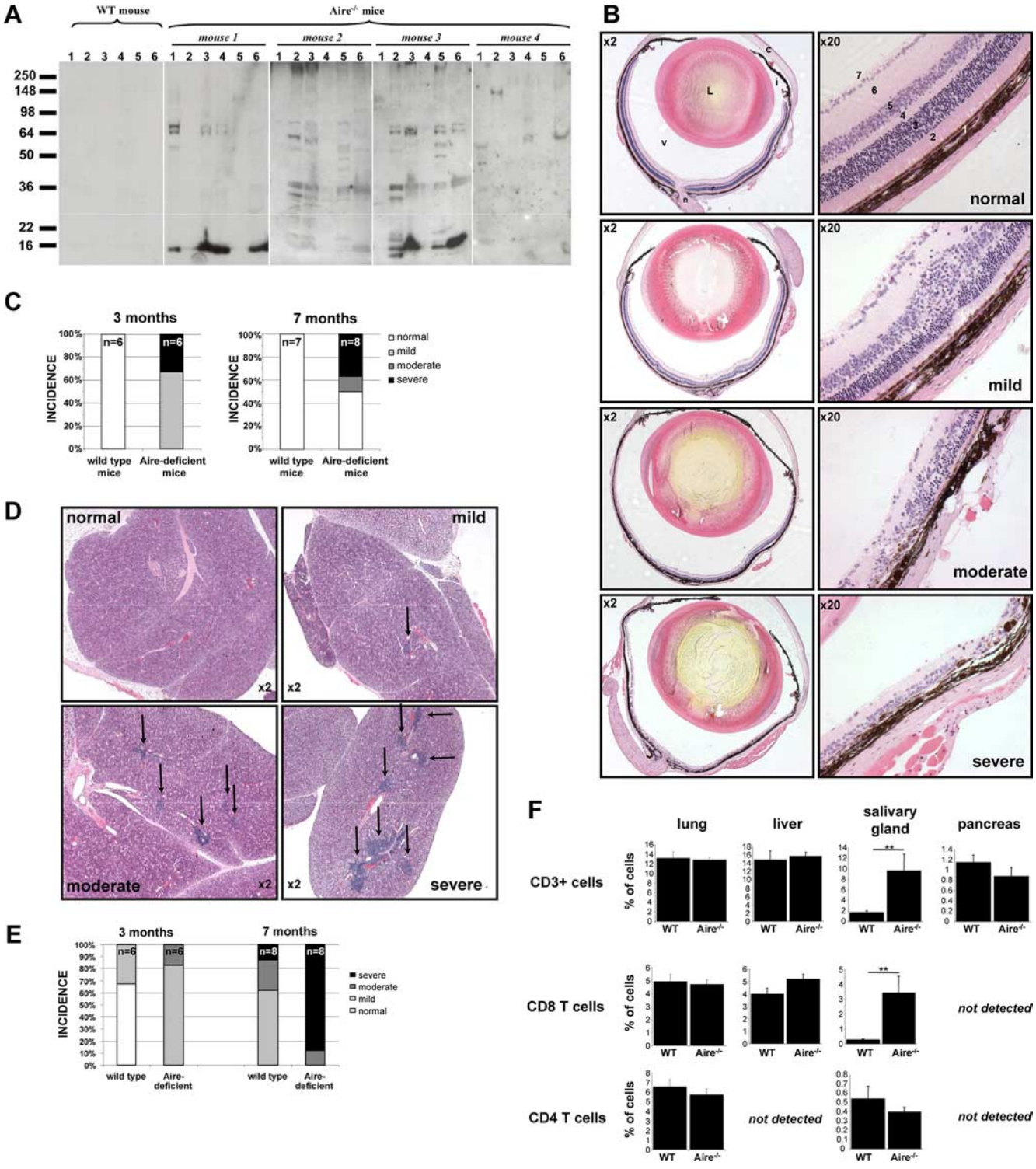

FIGURE 6. Evidence of autoimmunity in Aire-deficient mice. *A*, Autoantibodies generated in Aire-deficient mice. Each lane of the immunoblot shows autoantibodies in the serum from 20- and 25-wk-old individual Aire KO mice or from a WT mouse immunoblotted against testis (1), lung (2), salivary gland (3), liver (4), eye (5), and pancreas (6) Ags. *B*, Eye and retinal sections, showing uveoretinitis in Aire-deficient mice, reveal development of spontaneous autoimmunity in eyes. Tissue sections from WT and Aire-deficient mice are stained with H&E. The images show the different severity grade observed in each group of mice: normal (no disease), mild (sporadic infiltration), moderate (clear infiltrate with many foci), and severe (many extensive areas of infiltration). Marked as: l, lens; c, cornea; i, iris; r, retina; n, optic nerve; v, vitreous; 1, pigmented epithelium; 2, photoreceptor layer; 3, outer nuclear layer; 4, outer plexiform layer; 5, inner nuclear layer; 6, inner plexiform layer; 7, ganglion cell layer and inner limiting membrane. *C*, The graph gives an overview of frequency and severity of autoimmunity in the eye. *D*, Salivary gland sections, showing infiltration (arrows) in Aire-deficient mice, reveal development of spontaneous autoimmunity in submandibular glands. Tissue sections from WT and Aire-deficient mice are stained with H&E. The images show the different severity grade observed in each group of mice: normal (no disease), mild (sporadic infiltration), moderate (clear infiltrate with many foci), and severe (many extensive areas of infiltration). *E*, Overview of frequency and severity of autoimmunity in the salivary gland. *F*, Proportion of the T cell subsets in the lung, liver, salivary gland, and pancreas from 12 WT and 12 Aire-deficient mice.

To more specifically monitor alterations in the TCR repertoire, we analyzed variations in both length and distribution of the most variable region of the TCR Vβ-chain, the CDR3. For this we used a RT-PCR approach that subdivides a bulk CD4$^+$ T cell population (i.e., from thymus, spleen, lymph nodes) based on rearranged Vβ/Jβ gene segments and the resulting length of the TCR's third CDR (CDR3). This technique, referred to as immunoscope analysis (31), has the potential to identify clonal expansions. It allows identification of modifications in the CDR3 length Gaussian distribution patterns typically observed in WT animals. These CDR3 length alterations observed in some Vβ families can be visualized graphically (Fig. 5*B*), allowing global assessment of total Vβ alterations in each sample. In our case, only Gaussian distributions were observed in both WT and Aire$^{-/-}$ mice, as illustrated by the profiles of the major Vβs of CD4$^+$ T cells (Fig. 5*B*), suggesting polyclonal expansion. Thus, no obvious oligoclonal expansions dominated the repertoire of Aire$^{-/-}$ mice. Using these data, Fig. 5*C* shows the percentage perturbation of different CDR3 lengths for each Vβ (difference between the normalized WT profile and the sample for each CDR3 length). This analysis confirmed that the variation was generally low (i.e., $<$10%). Occasionally, greater alterations of between 10% and 30% were observed, but these were not reproducibly found in every Aire$^{-/-}$ mouse. The exception to this was Vβ18, which was perturbed by $>$10% in all Aire$^{-/-}$ thymi, but not in the other lymphoid organs. As a generalization, these results suggest that each individual Aire$^{-/-}$ mouse developed its own polyclonal repertoire of autoreactive T cells.

Classic and major autoantibodies found in APECED are not present in Aire-deficient mice

APECED patients have high levels of serum Abs reacting specifically with components in the affected organs. A number of the autoantigens, which are predominantly intracellular enzymes, have been identified such as ATP4a, CYP17, CYP21, CYP11A1, CYP1A2, and GAD65 (summarized in Ref. 42). Radioimmunoassay was used to screen Aire-deficient mice for the presence of autoantibodies against mouse Gad65, Cyp1a2, insulin, Atp4a, enolases, and Hsp90 with negative results (data not shown). Recently, high-titer neutralizing IgG autoantibodies reactive to most IFN-α subtypes have been found in APS1 patients (20, 43). Sera from 33 Aire-deficient mice and 12 normal mice were therefore screened for the presence of such autoantibodies to Mu-IFN-α but, in contrast to a rat anti-Mu-IFN-α mAb with a neutralizing titer of 1280, none of these sera was positive (titer $<$40). This suggests that Aire-deficient mice do not have the same autoantibody pattern as do human patients.

Expression of APECED autoantigens in Aire-deficient mTEC

Several studies have shown a correlation between loss of intrathymic expression of certain TSAs and the development of autoimmunity targeted toward these Ags (4, 44–46). However, Aire-deficient mice can also develop autoimmunity against Ags whose intrathymic expression is unaltered in the absence of Aire (19, 23). To determine whether the autoantigens commonly targeted in APECED patients were Aire activation targets, Affymetrix expression arrays were performed on WT and Aire$^{-/-}$ mTEC. Results show that *Nalp5, Cyp11a1, Ins2, Th*, and *Pah* were significantly down-regulated in Aire$^{-/-}$ mTEC, with the 3.9-fold reduction in expression of *Pah* being the largest significant fold change observed (Table I). Quantitative real-time RT-PCR was employed to confirm Affymetrix results for these lowly expressed TSA genes. Results confirmed the significant down-regulation of *Nalp5, Cyp11a1, Th, Pah* and *Ins2* in Aire$^{-/-}$ mTEC (Table I). However, *Gad2* and *Cyp1a2* were only found to be down-regulated in Aire$^{-/-}$ mTEC by quantitative RT-PCR. Taken together, these results suggest that Aire controls the expression of some, but not all, of the genes whose products are commonly targeted Ags in APECED patients.

Infertility is highly prevalent in male Aire-deficient mice

Infertility problems have been described in human APECED disease with a high prevalence in females (60% vs 14% of males) (1). The infertility problems previously noticed in Aire-deficient mice (3, 19, 22) were also observed in our Aire-deficient mice. Indeed, when intercrossed, Aire-deficient mice failed to produce any litters. Interestingly, this issue was most often the result of a fertility defect in the Aire-deficient males and not in the females. To confirm their sterility, we assessed the quality and the capacity of sperm from Aire-deficient mice to fertilize an oocyte via in vitro fertilization. We observed a 73% fertilization success rate with Aire-deficient sperm compared with 93% for a WT sperm. Of particular note, there was significant mouse-to-mouse variation in the quality (as indicated by mobility parameters and ultimately reflected in fertilization rates) and quantity of sperm retrieved from our Aire$^{-/-}$ males. This leads us to suspect the presence of anti-sperm Abs. The testis histology of Aire$^{-/-}$ mice was qualitatively identical to that of WT mice. At the ages observed, there were no differences in testis weights between genotypes.

Autoantibodies are detected against different organs

Although we observed only a minor increase in activated CD4$^+$ T cells, slight perturbations to the Vβ repertoire, and no autoantibodies against the known major targets in APECED, we analyzed autoantibody production against antigenic tissue proteins by our Aire-deficient mice. Characteristically, sera of APECED patients contain specific autoantibodies indicative of an ongoing autoimmune response against target organs. To investigate the range and the specificity of the autoantibodies elicited by the Aire deficiency, we probed immunoblots of protein extracts from several tissues (testis, lung, liver, salivary gland, eye, and pancreas) with sera from individual Aire-deficient mice (Fig. 6*A*). These analyses revealed sporadic and distinct patterns for each mouse, with some common bands. While sera from mice 1 and 3 displayed strong reactivity against the liver and pancreas, mouse 1 also reacted to components of testis and salivary gland, whereas mouse 3 reacted to proteins from the lung and eye. Interestingly, sera from all four mice had autoantibodies against liver and pancreas, while three reacted against testis, lung, salivary gland, and eye. Despite the presence of autoantibodies against the pancreas in all four Aire$^{-/-}$ mice, diabetes was not detected in any of these animals (data not shown). Taken together, these results showed that even Aire$^{-/-}$ mice of the same genetic background develop autoimmunity against different organs and autoantigens. These data provide a potential explanation for the observed mouse-to-mouse variations in male fertility with the presence of anti-testis Abs in the serum.

Histology

To confirm the development of autoimmunity in Aire-deficient mice, histological analysis was performed on several organs, including salivary glands and eyes, of 3- and 7-mo-old mice. It has been shown that Aire-deficient mice develop a spontaneous autoimmune uveitis that increases in frequency and severity with age and is characterized by mononuclear infiltrate and autoantibodies specific to the photoreceptor layer of the retina (3, 44). The same observations were made in our Aire-deficient mice. Indeed, irrespective of age, uveoretinitis was present in most Aire-deficient mice but not in WT mice, with severe retinal destruction in 40% of animals (Fig. 6, *B* and *C*). A mild phenotype was observed in most

Table I. *Expression of APECED autoantigens in Aire-deficient mTEC*[a]

			Affymetrix Array				Quantitative RT-PCR				
KO vs WT	Symbol	Name	Avg. Log Expr.	FC	FDR	*p*	FC	FDR	*p*	Human APECED Manifestation	Tissue Affected
Endocrine	Nalp5	NACHT, leucine-rich repeat and PYD containing 5	2.4	−2.7	0.03	*	−82.5	8.93×10^{-8}	***	Hypoparathyroidism	Parathyroid glands
	Cyp21a1	Cytochrome P450, family 21, subfamily a, polypeptide 1	3.0	1.2	0.36		−1.7	0.41		Addison's disease	Adrenal gland
	Cyp17a1	Cytochrome P450, family 17, subfamily a, polypeptide 1	4.1	−1.1	0.52		−1.8	0.36			
	Cyp11a1	Cytochrome P450, family 11, subfamily a, polypeptide 1	3.4	−1.6	0.02	*	−92.8	6.79×10^{-8}	***		
	Tpo	Thyroid peroxidase	2.8	−1.2	0.36		Not detected			Hypothyroidism	Thyroid gland
	Tgn	Thyroglobulin	2.7	1.0	0.86		2.2	0.25			
	Gad1	Glutamic acid decarboxylase 1	6.3	1.4	0.52		−1.6	0.49		Type I diabetes	Pancreas
	Gad2	Glutamic acid decarboxylase 2	2.3	1.2	0.36		−12.7	2.93×10^{-4}	***		
	Ica1	Islet cell autoantigen 1	4.6	1.3	0.16		Not done				
	Ptprn2	Protein tyrosine phosphatase, receptor type, N polypeptide 2	3.1	1.2	0.36		Not done				
	Ptprn	Protein tyrosine phosphatase, receptor type, N	3.3	1.2	0.36		−2.9	0.12			
	Ins1	Insulin I	3.6	1.1	0.55		Not done				
	Ins2	Insulin II	6.2	−2.0	0.02	*	−818.8	2.63×10^{-11}	***		
	Cyp17a1	Cytochrome P450, family 17, subfamily a, polypeptide 1	4.1	−1.1	0.52		−1.8	0.36		Gonadal failure	Ovary, testis
	Cyp11a1	Cytochrome P450, family 11, subfamily a, polypeptide 1	3.4	−1.6	0.02	*	−92.8	6.79×10^{-8}	***		
Non endocrine	Sox9	SRY-box containing gene 9	7.0	1.3	0.36		2.2	0.25		Vitiligo	Skin
	Sox10	SRY-box containing gene 10	4.0	1.2	0.36		−3.8	0.05			
	Th	Tyrosine hydroxylase	3.1	−1.7	0.03	*	−37.9	2.31×10^{-6}	***	Alopecia	Scalp
	Tph1	Tryptophan hydroxylase 1	6.1	1.2	0.81		1.1	0.93		Malabsorption	Intestine
	Tph2	Tryptophan hydroxylase 2	1.4	−1.2	0.52		Not done				
	Hdc	Histidine decarboxylase	8.2	1.2	0.83		1.3	0.67			
	Cyp1a2	Cytochrome P450, family 1, subfamily a, polypeptide 2	3.5	−2.9	0.09		−3265.8	1.10×10^{-12}	***	Autoimmune hepatitis	Liver
	Cyp1a1	Cytochrome P450, family 1, subfamily a, polypeptide 1	3.2	−1.2	0.48		Not done				
	Cyp2a5	Cytochrome P450, family 2, subfamily a, polypeptide 5	8.6	−8.0	0.07		Not done				
	Ddc	Dopa decarboxylase	5.2	−2.7	0.06		−2.6	0.17			
	Pah	Phenylalanine hydroxylase	8.1	−3.9	0.01	**	−6.4	0.01	**		
	Atp4a	ATPase, H^+/K^+ transporting, α polypeptide	5.8	−3.0	0.20		−2.7	0.15		Autoimmune gastritis	Stomach
	Atp4b	ATPase, H^+/K^+ transporting, β polypeptide	4.9	−1.2	0.36		−2.1	0.27			

[a] Affymetrix array datas and quantitative RT-PCR are presented according to their fold change (FC) and false discovery rate (FDR).
*, $p < 0.05$; **, $p < 0.01$; ***, $p < 0.001$.

Aire-deficient mice with distortion of the outer and inner nuclear layer and a reduction in size of the photoreceptor layer (Fig. 6, *B* and *C*). In some cases, vitritis was also found in Aire-deficient mice (data not shown).

Salivary glands consist of exocrine tissue whose main function is to secrete saliva, thereby keeping the mouth and other parts of the digestive system moist (47). Aire-deficient mice have been reported to exhibit extensive lymphocytic infiltration of salivary and lacrimal glands and destruction of epithelial cells (3, 19), as seen in primary Sjögren's syndrome (48). The histological phenotype in the submaxillary gland was ranked according to four degrees of severity (Fig. 6*D*). Analysis of the extent of the infiltration

in our Aire-deficient mice showed more severe infiltration than that seen in normal mice (Fig. 6*E*). We also observed an effect of age on the degree of lymphocytic infiltration of exocrine tissues. Moreover, when we analyzed the parotid and sublingual glands in Aire-deficient mice, we observed sporadic infiltration in the sublingual gland (40% in Aire$^{-/-}$ mice vs 0% in WT mice), while most Aire-deficient mice analyzed showed severe infiltration in the parotid gland (80% in Aire$^{-/-}$ mice vs 0% in WT mice) (data not shown). The pancreas, liver, stomach, kidney, epididymis, thyroid, parathyroid, testis, ovary, and epidermis, also affected in APECED disease, appeared histologically normal in our Aire-deficient mice (data not shown). Flow cytometry experiments revealed an abnormal infiltration by activated CD69$^+$ and CD44$^+$ CD8$^+$ T cells in the salivary glands of Aire-deficient mice, but not in the lungs, liver, or pancreas (Fig. 6*F*).

Aire-deficient mice are not susceptible to Candida *infection*

APECED patients develop candidiasis (1), an infection caused by the fungus *C. albicans*, usually before 5 years of age, with the nails, skin, tongue, and mucous membranes being the major sites of infection. Additionally, the role of neutralizing IgG autoantibodies reactive to most IFN-α subtypes in APS1 syndrome is also unclear. One interesting possibility was a potential link between these autoantibodies and the propensity to develop susceptibility to *Candida* infections in these patients, as suggested by Meager et al. (43). We tested the susceptibility of our Aire-deficient mice to *C. albicans* after oral or systemic infection. In Fig. 7, we show that Aire-deficient mice respond equivalently to WT mice to oral *Candida* infection, irrespective of whether mice were young (1 wk) or old (11–14 mo). The same observations were made for systemic infection (data not shown).

Discussion

AIRE is an important transcription regulator that mediates a role in central tolerance in part by promoting the promiscuous expression of tissue-specific Ags in the thymus, although other contributions have been implicated (49). We have disrupted the first PHD domain at exon 8 of Aire to reflect the 13-bp deletion of human APECED patients (the second most frequently observed mutation) to examine the role of Aire in central tolerance in the mouse. While this disruption in the Aire gene clearly altered the development of mTEC, it resulted in minimal changes to the T cell repertoire and only mild autoimmune manifestations, in agreement with other reports of Aire-deficient mice (3, 19, 20).

The impact of this new model of Aire-deficient mice is important for several reasons, which are summarized in Tables II and III. First, these mice, although deficient for Aire, retain the expression of a truncated Aire-β-gal fusion as demonstrated by anti-β-gal staining, whereas the expression of mutant Aire protein in other Aire-deficient mice was not detected by the founding laboratories (3, 22). Dooley et al. recently used a goat polyclonal anti-AIRE Ab raised against an "internal peptide" of human AIRE to implicate expression of a truncated Aire protein in Peltonen's Aire-deficient mice (50), but whether this will achieve independent verification using other approaches must await future studies. Irrespective of such unresolved issues, our stable mutant protein, which contains the integral HSR, nuclear localization signal (NLS), SAND, and truncated PHD1 domains, closely emulates the common 13-bp deletion in human APECED patients for which several studies strongly suggest the expression of a stable truncated protein (27–29). Second, the targeting vector used in the deletion of exon 6 and premature termination of the Aire protein at the end of the SAND domain in Peltonen's mice has a selection cassette that was not removable, raising the possibility of affecting the expression of neighboring genes (51–57). Third, our model allows previously unappreciated insights into the role of Aire in the maintenance of normal fertility. Specifically, a high prevalence of infertility is observed in our Aire$^{-/-}$ males, whereas in Peltonen's mice, 44% of Aire$^{+/-}$ and 85% of Aire$^{-/-}$ mice, both males and females, are infertile (22). Within humans, 60% of female APECED patients and 14% of males develop gonadal failure, and carriers are apparently phenotypically normal (1). For the males at least, data presented herein raise the possibility that anti-sperm Abs interfere with sperm function at fertilization but do not result in epididymitis and orchitis, at least at the ages examined. Note, however, that within men, the reported gonad failure may be a secondary consequence of systemic illness (reviewed in Ref. 58) or as a consequence of the immunoneutralization of major components of the steroidogenic pathway, for example,17HSBD3 (59) and SRD5A2 (60). Alternatively, this sterility could be simply due to low levels of Aire expression in testis (61). Finally, whereas other Aire-deficient mice have been generated on a mixed genetic background and then backcrossed to a specific background for few generations, our mice were generated as pure C57BL/6 by using C57BL/6 embryonic stem (ES) cells (Table II), perhaps explaining the phenotypic differences observed (Table III). This is strongly supported by reports that showed the effect of a congenic "footprint" (62, 63). Indeed, the mouse phenotype that is derived from 129 ES cells is different from mice derived from C57BL/6 ES cells, even if backcrossed to C57BL/6. The remaining congenic genomic regions of 129 maintain the 129-related phenotype.

Our Aire-deficient mice have 4-fold more mature mTEC (MHC-II^{high}Ly51^{low}CD45$^-$) than do WT littermates. A similar observation was made by Anderson et al., who showed a 2-fold increase in the number of mTEC (phenotyped according to the expression of CDR1 and CD80 on CD45$^-$Epcam$^+$ cells) in their Aire-deficient mice (3). The difference observed between these two models could be dependent on any of the kind of Aire mutation, genetic background, and staining criteria used. Although the total number of mTEC remained constant, as previously reported (22), we confirm the important difference in the ratio of mature-to-immature mTEC, where CD45$^-$MHC-II^{low}Ly51^{low} cells are considered as immature (64). As Aire is expressed by the mature mTEC, increased numbers of mature mTEC in Aire$^{-/-}$ mice could reflect a homeostatic effect within a niche that can only accommodate a finite number of mTEC (whether immature or mature). This latter possibility might be the case if Aire regulates the expression of genes necessary to detect the presence of mature mTEC or if Aire expression limits the survival of mature mTEC. As recently suggested by Gray et al. (64), Aire$^{-/-}$ mature mTEC show a potential capacity to survive better than do WT mature mTEC. This is also suggested by our gene profiling analysis of WT vs Aire$^{-/-}$ mature mTEC, where an increased expression of antiapoptotic molecules and a down-regulation of proapoptotic molecules are observed in Aire-deficient mTEC (F.-X. Hubert and H. S. Scott, unpublished observations). Although Gillard et al. (41) recently showed a reduction in the size of the medulla in Aire-deficient mice, we and others (3, 22, 23) were unable to detect morphological abnormalities in the thymus.

Aire-deficient mice do develop autoimmune symptoms, although mild in severity, with increased numbers of activated CD4$^+$ T cells and autoantibodies (3, 22, 23). It is possible that the increase in activated CD4 T cells is caused by overrepresentation of certain T cells that are normally destined for negative selection. Analyses of the TCR repertoire via both length and distribution of the most variable region of the TCR Vβ-chain (CDR3) in bulk CD4$^+$ T cell populations revealed only slight skewing in the distribution of CDR3 length within each Vβ. Differences in small

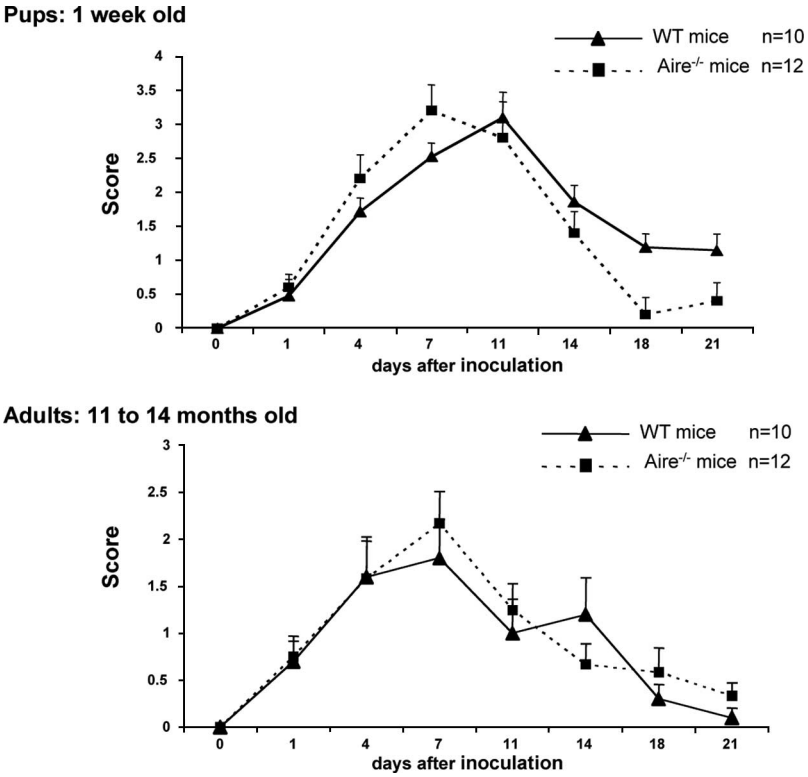

FIGURE 7. Aire-deficient mice are not susceptible to oral infection of *C. albicans*. Oral infection with *C. albicans* 3630 in Aire-deficient mice and WT mice. Data points represent the score (mean ± SEM) for a minimum 10 mice per time point in each group. All experiments were repeated at least once for pups and three times for adults.

subpopulations of autoreactive $CD4^+$ T cells, however, may be hidden within the pool of bulk $CD4^+$ T cells, particularly in the thymus, where Aire negative selection occurs in the relatively later stage during thymocyte development and therefore may be difficult to discriminate by these techniques. Ramsey et al. performed similar repertoire analysis, but on whole thymus and spleen, and while few differences were found, they identified changes within the Vβ18, Vβ19, and Vβ20 repertoires of the spleen (22). However, their experimental design did not distinguish between CD4 and CD8 T cells, making interpretation difficult. Analysis of the T cell repertoire within affected organs will perhaps provide better information on the repertoire of infiltrating autoreactive T cells. Aire deficiency within the mTEC compartment does not seem to greatly perturb T cell education, with the absolute number and proportion of $CD4^+$ T cells, $CD8^+$ T cells, and regulatory T cells remaining the same in $Aire^{-/-}$ mice (3, 6, 19, 23). This does not, however, exclude the possibility that differences in the repertoire of regulatory T cells could contribute to autoimmune disease in our Aire-deficient mice.

Although Aire-deficient mice develop autoantibodies, it is clear that the mice do not have the same autoantibody pattern as do human patients (ATP4a, CYP17, CYP21, CYP11A1, CYP1A2, GAD65, anti-type I IFN) (21). This is in agreement with the fact that none of the disease components typical for APECED has been described in the Aire-deficient mice. Indeed, one of the first symptoms that typically appear during early childhood in APECED patients, chronic mucocutaneous candidiasis, is not found in Aire-deficient mice, notably reinforced by the absence of anti-enolase Abs, which target an immunodominant Ag of the opportunistic pathogen *C. albicans*. This may be also linked to the absence, in mice, of anti-IFN-α autoantibodies, seen in humans (43). Our $Aire^{-/-}$ mice share a similar mild autoimmune phenotype to other reported Aire-deficient mouse models, which is considerably less severe than that of APECED patients and is dependent on genetic background (19, 20). It has been proposed that this is consistent with the idea that Aire controls an alternative set of genes in humans and mice (21). Given the lack of data from APECED patient mTEC to compare with Aire KO knockout

Table II. *The different Aire-deficient mice*

	Peltonen's Mice	Mathis's Mice	Matsumoto's Mice	Scott's Mice
mRNA				
Targeted exon(s)	Exon 6	Exon 2	Exons 5–12	Exon 8
Targeted protein domain(s)	SAND	HSR	SAND, PHD1, PRR, PHD2	PHD1
Predicted mRNA	Exons 1–5	Exon 1	Exons 1–4	Exons 1–7
Protein				
Predicted protein domains	HSR, NLS, premature SAND	Premature HSR	HSR, NLS	HSR, NLS, SAND, premature PHD1
Expression	No	No	?	Truncated
Localization			?	Mainly nuclear but also cytoplasmic
ES strain → blastocyte strain	J129 → C57BL/6	SV129 → C57BL/6	TT2	C57BL/6 → C57BL/6
Major human conterpart mutation	R257X			d1094-1106 del13

Table III. *Summary of the findings made in the different Aire-deficient mice*

	Peltonen's mice						Mathis's mice							Matsumoto's mice		Scott's mice
strain	C57BL/6	C57BL/6	C57BL/6	C57BL/6	C57BL/6	C57BL/6	C57BL/6	C57BL/6	NOD and BALB/c	C57BL/6J	BALB/cJ	NOD/LtJ	SJL/J	C57BL/6 (mixed background)	NOD/Shi Jic	C57BL/6
generation analysed	gen?	gen?	F6	gen?	F2	F6	F2/F3	F3/F4		> 8 gen	> 8 gen	> 8 gen	> 8 gen	gen?	F6 to F9	
thymic epilthelial cells							increase twice								normal	increase 4 times
thymus: morphology	no altered morphology, atrophy 42%		increase B cells	contracted medullary compartment										normal	normal	not alterated morphology
thymic selection					negative selection defect of SP CD4 T cells	positive selection defect		negative selection defect of SP CD4 and CD8 T cells								
T/B cells	normal distribution excepted in LN twice, alteration of TCR repertoire V18, V19 & V20	normal capacity to proliferate					Increased activation/ memory markers on CD4 T cells	normal Treg number							normal number of B220, CD3, CD4, foxp3 and CD8 cells in the spleen, cell surface markers (CD25, CD62L,CD69) unchanged on CD4 T cells but CD44 is increased	normal T reg, increased activation/memory markers, few alteration of the repertoire
Autoanti-bodies (% of affected)	liver (20%), testis (54%), pancreas (47%), adrenal (20%)									pancreas (0%), eyes (84%), SG (10%), stomach (0%), ovary (16%)	pancreas (0%), eyes (33%), SG (0%), stomach (100%), ovary (0%)	pancreas (100%), eyes (100%), SG (100%), stomach (67%), ovary (33%)			pancreas (100%), stomach (100%), kidney (100%), liver (100%)	testis (50%), lung (75%), SG (100%), liver (75%), eyes (75%), pancreas (100%)
sera test		negative against: 21-OH, 17-OH, TPH, P450scc, AADC, Gad65, IA2, Cyp1a2, ANA							auto-Abs against mucin 6					auto-Abs against a-fodrin		negative against: Gad65, Cyp1a2, Insulin, Atp4a, enolase I, II, III, Hsp90, anti-type I IFN
histology: infiltration (% of affected)	liver (50%), pancreas (0%), thyroid (0%) no adrenal gland		pancreas, lung, adrenal, thyroid, and ovary, with the highest frequency observed in the liver and lung				thyroid (35%), retina (65%), stomach (35%), ovary (77%), pancreas (65%)			eyes (67%), stomach (9%), SG (100%), lung (36%), prostate (100%), liver (0%), ovary (0%), pancreas (0%), thyroid (0%)	eyes (80%), stomach (100%), SG (20%), lung (50%), liver (40%), prostate (100%), ovary (100%), pancreas (0%), thyroid (0%)	eyes (93%), stomach (87%), SG (100%), lung (100%), liver (86%), prostate (100%), ovary (88%), pancreas (100%), thyroid (54%)	eyes (0%), stomach (100%), SG (100%), lung (100%), liver (83%), prostate (100%), ovary (50%), pancreas (71%), thyroid (0%)	SG (100%), lacrymal gland (100%), stomach (10%), pancreas (10%), thyroid (0%), heart (0%), lung (0%), liver (0%), kidney (0%), small intestine (0%), testis (0%), ovary (0%)	pancreas (81%) destruction acinar cell but not b-islets, liver (92%), lung (96%), confirmed infiltration in SG, thyroid, prostate	eyes (80%), parotid gland (80%), sublingual gland (40%), pancreas (0%), epidermis (0%), liver (0%), stomach (0%), kidney (0%), epididymus (0%), thyroid (0%), parathyroid (0%), testis (0%), ovary (0%)
fertility problem	yes (85%) same ratio for male and female													yes, both male and female Aire-/- mice are fertile when crossed with WT mice, homozygous crossing produced offspring only occasionally		yes, only males are subfertile
Spontaneous candidiasis																no
Susceptibility to candidiasis																no
Reference	Ramsey et al, Hum. Mol. Genet. 2002	Pontynen et al, J. Autoimmun. 2006	Hassler et al, Blood 2007	Gillard et al, J.Immunol. 2007	Liston et al, Nat. Immunol. 2003	Li et al, PNAS 2007	Anderson et al, Science 2002	Anderson et al, Immunity 2005	Gavanescu et al, PNAS 2007	Jiang et al, J. Exp. Med. 2005				Kuroda et al, J. Immunol. 2005	Niki et al, J. Clin. Invest. 2006	in this paper

SP indicates single positive; SG, salivary gland.

mTEC, this fundamental question will be difficult to answer. However, comparisons of human and mouse WT mTEC suggest that human and mouse AIRE/Aire do share similar targets (46, 65, 66).

Table I shows that many of the orthologous genes putatively controlled by AIRE in human thymus, which then become autoantigens in APECED, are also controlled by Aire in mice. The questions are, why, if the orthologous TSAs, such as Nalp5 and Cyp11a1, are controlled by AIRE/Aire in the mTEC of both humans and mice, is the phenotype so different in mice, and why do we fail to observe autoimmune reactivity associated with these TSAs, particularly autoantibodies and tissue infiltration (hypoparathyroidism and Addison's disease (adrenal cortex), respectively)? Is it that other TSAs for that tissue, such as Cyp21a1 and Cyp17a1 of the adrenal cortex, are controlled by AIRE in the human mTEC but not by Aire in mouse mTEC? Does this limit the pathological autoimmune damage by multiple autoantibodies and autoreactive T cells to a target tissue or organ?

We know that the disease has a stochastic element, as the phenotype can be different between human twins (26) and patients from human genetic isolates with the same genotype (25). Similarly, there is considerable variation between isogenic mouse siblings. This would normally suggest an environmental effect. However, twins, genetic isolates, and mouse siblings share largely common environments. Thus, the stochastic nature of the disease in both humans and mice points to another factor. Perhaps stochastic epigenetic regulation is the smoking gun (67).

We need to separate the causes for difference in phenotype between isogenic siblings (humans and mice) from the difference in phenotypes between human APECED and mouse Aire knockouts. Epigenetics and even limited environmental differences may explain the phenotypic differences between isogenic siblings (humans and mice). Aire knockout mice phenotypes differ enormously when put on different genetic backgrounds (Table III and Refs. 20, 23). The huge differences between human APECED and the several mouse Aire knockout phenotypes could still be genetic background, affecting not only direct Aire targets, but also functions throughout the immune system such as peripheral tolerance, inflammation control, and innate immunity.

Taken together, our observations suggest that our Aire-deficient mice do show some autoimmunity that mimics human APECED, and thus these mice provide a good mechanistic model for dissecting the process of APECED. All of our Aire-deficient mice present with subfertility, organ infiltration, circulating autoantibodies, activated T cells, and few alterations in the repertoire of peripheral T cells. These observations support the view that both genetic and environmental factors contribute substantially to the overt nature of autoimmunity associated with Aire mutations, even for mutations identical to those found in humans with APECED. Although some genetic studies did not find susceptible HLA on APECED patients, our study and others cannot exclude a role for the MHC (49) in the symptoms and severity of disease in Aire-deficient mice. Interestingly, these studies have shown consistently that the phenotype of C57BL/6 Aire-deficient mice is surprisingly mild.

Acknowledgments

The LacZ-LoxP-Neo-PGK-LoxP cassette was a gift from Drs. Yann Hérault and Denis Duboule (University of Geneva). We thank Edouard G. Stanley and other members of the Genetically Modified Mouse Laboratory at the Walter and Eliza Hall Institute (WEHI) and WEHI Animal Services for animal care and management, Dr. Robert Ashman of the School of Dentistry, University of Queensland (Brisbane, Queensland, Australia) for the *C. albicans* isolate and protocols, and Dr. L. Gabriel Sanchez-Partida for help with the fertility analysis. Affymetrix GeneChips were performed by the Australian Genome Research Facility, which was established through the Commonwealth-funded Major National Research Facilities program, and we thank Dr. Ken Simpson for help in analysis and Belinda Phipson for depositing the array data on the GEO public database.

Disclosures

The authors have no financial conflicts of interest.

References

1. Ahonen, P., S. Myllarniemi, I. Sipila, and J. Perheentupa. 1990. Clinical variation of autoimmune polyendocrinopathy-candidiasis-ectodermal dystrophy (APECED) in a series of 68 patients. *N. Engl. J. Med.* 322: 1829–1836.
2. Nagamine, K., P. Peterson, H. S. Scott, J. Kudoh, S. Minoshima, M. Heino, K. J. Krohn, M. D. Lalioti, P. E. Mullis, S. E. Antonarakis, et al. 1997. Positional cloning of the APECED gene. *Nat. Genet.* 17: 393–398.
3. Anderson, M. S., E. S. Venanzi, L. Klein, Z. Chen, S. P. Berzins, S. J. Turley, H. von Boehmer, R. Bronson, A. Dierich, C. Benoist, and D. Mathis. 2002. Projection of an immunological self shadow within the thymus by the aire protein. *Science* 298: 1395–1401.
4. Liston, A., S. Lesage, J. Wilson, L. Peltonen, and C. C. Goodnow. 2003. Aire regulates negative selection of organ-specific T cells. *Nat. Immunol.* 4: 350–354.
5. Liston, A., D. H. Gray, S. Lesage, A. L. Fletcher, J. Wilson, K. E. Webster, H. S. Scott, R. L. Boyd, L. Peltonen, and C. C. Goodnow. 2004. Gene dosage-limiting role of *Aire* in thymic expression, clonal deletion, and organ-specific autoimmunity. *J. Exp. Med.* 200: 1015–1026.
6. Anderson, M. S., E. S. Venanzi, Z. Chen, S. P. Berzins, C. Benoist, and D. Mathis. 2005. The cellular mechanism of Aire control of T cell tolerance. *Immunity* 23: 227–239.
7. Aschenbrenner, K., L. M. D'Cruz, E. H. Vollmann, M. Hinterberger, J. Emmerich, L. K. Swee, A. Rolink, and L. Klein. 2007. Selection of $Foxp3^+$ regulatory T cells specific for self antigen expressed and presented by $Aire^+$ medullary thymic epithelial cells. *Nat. Immunol.* 8: 351–358.
8. Heino, M., P. Peterson, J. Kudoh, K. Nagamine, A. Lagerstedt, V. Ovod, A. Ranki, I. Rantala, M. Nieminen, J. Tuukkanen, et al. 1999. Autoimmune regulator is expressed in the cells regulating immune tolerance in thymus medulla. *Biochem. Biophys. Res. Commun.* 257: 821–825.
9. Blechschmidt, K., M. Schweiger, K. Wertz, R. Poulson, H. M. Christensen, A. Rosenthal, H. Lehrach, and M. L. Yaspo. 1999. The mouse *Aire* gene: comparative genomic sequencing, gene organization, and expression. *Genome Res.* 9: 158–166.
10. Kogawa, K., S. Nagafuchi, H. Katsuta, J. Kudoh, S. Tamiya, Y. Sakai, N. Shimizu, and M. Harada. 2002. Expression of AIRE gene in peripheral monocyte/dendritic cell lineage. *Immunol. Lett.* 80: 195–198.
11. Halonen, M., M. Pelto-Huikko, P. Eskelin, L. Peltonen, I. Ulmanen, and M. Kolmer. 2001. Subcellular location and expression pattern of autoimmune regulator (Aire), the mouse orthologue for human gene defective in autoimmune polyendocrinopathy candidiasis ectodermal dystrophy (APECED). *J. Histochem. Cytochem.* 49: 197–208.
12. Lee, J. W., M. Epardaud, J. Sun, J. E. Becker, A. C. Cheng, A. R. Yonekura, J. K. Heath, and S. J. Turley. 2007. Peripheral antigen display by lymph node stroma promotes T cell tolerance to intestinal self. *Nat. Immunol.* 8: 181–190.
13. Gardner, J. M., J. J. Devoss, R. S. Friedman, D. J. Wong, Y. X. Tan, X. Zhou, K. P. Johannes, M. A. Su, H. Y. Chang, M. F. Krummel, and M. S. Anderson. 2008. Deletional tolerance mediated by extrathymic Aire-expressing cells. *Science* 321: 843–847.
14. Hubert, F. X., S. A. Kinkel, K. E. Webster, P. Cannon, P. E. Crewther, A. I. Proeitto, L. Wu, W. R. Heath, and H. S. Scott. 2008. A specific anti-Aire antibody reveals Aire expression is restricted to medullary thymic epithelial cells and not expressed in periphery. *J. Immunol.* 180: 3824–3832.
15. Pitkanen, J., V. Doucas, T. Sternsdorf, T. Nakajima, S. Aratani, K. Jensen, H. Will, P. Vahamurto, J. Ollila, M. Vihinen, et al. 2000. The autoimmune regulator protein has transcriptional transactivating properties and interacts with the common coactivator CREB-binding protein. *J. Biol. Chem.* 275: 16802–16809.
16. Uchida, D., S. Hatakeyama, A. Matsushima, H. Han, S. Ishido, H. Hotta, J. Kudoh, N. Shimizu, V. Doucas, K. I. Nakayama, et al. 2004. AIRE functions as an E3 ubiquitin ligase. *J. Exp. Med.* 199: 167–172.
17. Org, T., F. Chignola, C. Hetenyi, M. Gaetani, A. Rebane, I. Liiv, U. Maran, L. Mollica, M. J. Bottomley, G. Musco, and P. Peterson. 2008. The autoimmune regulator PHD finger binds to non-methylated histone H3K4 to activate gene expression. *EMBO Rep.* 9: 370–376.
18. Ferguson, B. J., C. Alexander, S. W. Rossi, I. Liiv, A. Rebane, C. L. Worth, J. Wong, M. Laan, P. Peterson, E. J. Jenkinson, et al. 2008. AIRE's CARD revealed, a new structure for central tolerance provokes transcriptional plasticity. *J. Biol. Chem.* 283: 1723–1731.
19. Kuroda, N., T. Mitani, N. Takeda, N. Ishimaru, R. Arakaki, Y. Hayashi, Y. Bando, K. Izumi, T. Takahashi, T. Nomura, et al. 2005. Development of autoimmunity against transcriptionally unrepressed target antigen in the thymus of Aire-deficient mice. *J. Immunol.* 174: 1862–1870.
20. Jiang, W., M. S. Anderson, R. Bronson, D. Mathis, and C. Benoist. 2005. Modifier loci condition autoimmunity provoked by Aire deficiency. *J. Exp. Med.* 202: 805–815.
21. Pontynen, N., A. Miettinen, T. P. Arstila, O. Kampe, M. Alimohammadi, O. Vaarala, L. Peltonen, and I. Ulmanen. 2006. Aire deficient mice do not develop the same profile of tissue-specific autoantibodies as APECED patients. *J. Autoimmun.* 27: 96–104.
22. Ramsey, C., O. Winqvist, L. Puhakka, M. Halonen, A. Moro, O. Kampe, P. Eskelin, M. Pelto-Huikko, and L. Peltonen. 2002. Aire deficient mice develop

multiple features of APECED phenotype and show altered immune response. *Hum. Mol. Genet.* 11: 397–409.
23. Niki, S., K. Oshikawa, Y. Mouri, F. Hirota, A. Matsushima, M. Yano, H. Han, Y. Bando, K. Izumi, M. Matsumoto, et al. 2006. Alteration of intra-pancreatic target-organ specificity by abrogation of Aire in NOD mice. *J. Clin. Invest.* 116: 1292–1301.
24. Su, M. A., K. Giang, K. Zumer, H. Jiang, I. Oven, J. L. Rinn, J. J. Devoss, K. P. Johannes, W. Lu, J. Gardner, et al. 2008. Mechanisms of an autoimmunity syndrome in mice caused by a dominant mutation in Aire. *J. Clin. Invest.* 118: 1712–1726.
25. Heino, M., P. Peterson, J. Kudoh, N. Shimizu, S. E. Antonarakis, H. S. Scott, and K. Krohn. 2001. APECED mutations in the autoimmune regulator (AIRE) gene. *Hum. Mutat.* 18: 205–211.
26. Scott, H. S., M. Heino, P. Peterson, L. Mittaz, M. D. Lalioti, C. Betterle, A. Cohen, M. Seri, M. Lerone, G. Romeo, et al. 1998. Common mutations in autoimmune polyendocrinopathy-candidiasis-ectodermal dystrophy patients of different origins. *Mol. Endocrinol.* 12: 1112–1119.
27. Rinderle, C., H. M. Christensen, S. Schweiger, H. Lehrach, and M. L. Yaspo. 1999. AIRE encodes a nuclear protein co-localizing with cytoskeletal filaments: altered sub-cellular distribution of mutants lacking the PHD zinc fingers. *Hum. Mol. Genet.* 8: 277–290.
28. Bjorses, P., M. Halonen, J. J. Palvimo, M. Kolmer, J. Aaltonen, P. Ellonen, J. Perheentupa, I. Ulmanen, and L. Peltonen. 2000. Mutations in the AIRE gene: effects on subcellular location and transactivation function of the autoimmune polyendocrinopathy-candidiasis-ectodermal dystrophy protein. *Am. J. Hum. Genet.* 66: 378–392.
29. Ramsey, C., A. Bukrinsky, and L. Peltonen. 2002. Systematic mutagenesis of the functional domains of AIRE reveals their role in intracellular targeting. *Hum. Mol. Genet.* 11: 3299–3308.
30. Gray, D. H., A. P. Chidgey, and R. L. Boyd. 2002. Analysis of thymic stromal cell populations using flow cytometry. *J. Immunol. Methods* 260: 15–28.
31. Pannetier, C., M. Cochet, S. Darche, A. Casrouge, M. Zoller, and P. Kourilsky. 1993. The sizes of the CDR3 hypervariable regions of the murine T-cell receptor beta chains vary as a function of the recombined germ-line segments. *Proc. Natl. Acad. Sci. USA* 90: 4319–4323.
32. Yu, L., D. T. Robles, N. Abiru, P. Kaur, M. Rewers, K. Kelemen, and G. S. Eisenbarth. 2000. Early expression of antiinsulin autoantibodies of humans and the NOD mouse: evidence for early determination of subsequent diabetes. *Proc. Natl. Acad. Sci. USA* 97: 1701–1706.
33. Meager, A. 2002. Biological assays for interferons. *J. Immunol. Methods* 261: 21–36.
34. Kawade, Y. 1980. An analysis of neutralization reaction of interferon by antibody: a proposal on the expression of neutralization titer. *J. Interferon Res.* 1: 61–70.
35. Irizarry, R. A., B. M. Bolstad, F. Collin, L. M. Cope, B. Hobbs, and T. P. Speed. 2003. Summaries of Affymetrix GeneChip probe level data. *Nucleic Acids Res.* 31: e15.
36. Gentleman, R. C., V. J. Carey, D. M. Bates, B. Bolstad, M. Dettling, S. Dudoit, B. Ellis, L. Gautier, Y. Ge, J. Gentry, et al. 2004. Bioconductor: open software development for computational biology and bioinformatics. *Genome Biol.* 5: R80.
37. Smyth, G. K. 2004. Linear models and empirical Bayes methods for assessing differential expression in microarray experiments. *Stat. Appl. Genet. Mol. Biol.* 3: article 3.
38. Jones, R. L., T. J. Kaitu'u-Lino, G. Nie, L. G. Sanchez-Partida, J. K. Findlay, and L. A. Salamonsen. 2006. Complex expression patterns support potential roles for maternally derived activins in the establishment of pregnancy in mouse. *Reproduction* 132: 799–810.
39. Farah, C. S., S. Elahi, K. Drysdale, G. Pang, T. Gotjamanos, G. J. Seymour, R. L. Clancy, and R. B. Ashman. 2002. Primary role for $CD4^+$ T lymphocytes in recovery from oropharyngeal candidiasis. *Infect. Immun.* 70: 724–731.
40. Derbinski, J., J. Gabler, B. Brors, S. Tierling, S. Jonnakuty, M. Hergenhahn, L. Peltonen, J. Walter, and B. Kyewski. 2005. Promiscuous gene expression in thymic epithelial cells is regulated at multiple levels. *J. Exp. Med.* 202: 33–45.
41. Gillard, G. O., J. Dooley, M. Erickson, L. Peltonen, and A. G. Farr. 2007. *Aire*-dependent alterations in medullary thymic epithelium indicate a role for *Aire* in thymic epithelial differentiation. *J. Immunol.* 178: 3007–3015.
42. Peterson, P., and L. Peltonen. 2005. Autoimmune polyendocrinopathy syndrome type 1 (APS1) and AIRE gene: new views on molecular basis of autoimmunity. *J. Autoimmun.* 25(Suppl.): 49–55.
43. Meager, A., K. Visvalingam, P. Peterson, K. Moll, A. Murumagi, K. Krohn, P. Eskelin, J. Perheentupa, E. Husebye, Y. Kadota, and N. Willcox. 2006. Anti-interferon autoantibodies in autoimmune polyendocrinopathy syndrome type 1. *PLoS Med.* 3: e289.
44. DeVoss, J., Y. Hou, K. Johannes, W. Lu, G. I. Liou, J. Rinn, H. Chang, R. R. Caspi, L. Fong, and M. S. Anderson. 2006. Spontaneous autoimmunity prevented by thymic expression of a single self-antigen. *J. Exp. Med.* 203: 2727–2735.
45. Gavanescu, I., B. Kessler, H. Ploegh, C. Benoist, and D. Mathis. 2007. Loss of Aire-dependent thymic expression of a peripheral tissue antigen renders it a target of autoimmunity. *Proc. Natl. Acad. Sci. USA* 104: 4583–4587.
46. Alimohammadi, M., P. Bjorklund, A. Hallgren, N. Pontynen, G. Szinnai, N. Shikama, M. P. Keller, O. Ekwall, S. A. Kinkel, E. S. Husebye, et al. 2008. Autoimmune polyendocrine syndrome type 1 and NALP5, a parathyroid autoantigen. *N. Engl. J. Med.* 358: 1018–1028.
47. Young, J. A. 1979. Salivary secretion of inorganic electrolytes. *Int. Rev. Physiol.* 19: 1–58.
48. Talal, N. 1988. Sjögren syndrome and pseudolymphoma. *Hosp. Pract.* 23: 71–75.
49. Mathis, D., and C. Benoist. 2007. Yes, it does. *Nat. Rev. Immunol.* 7: 1.
50. Dooley, J., M. Erickson, and A. G. Farr. 2008. Alterations of the medullary epithelial compartment in the Aire-deficient thymus: implications for programs of thymic epithelial differentiation. *J. Immunol.* 181: 5225–5232.
51. Fiering, S., E. Epner, K. Robinson, Y. Zhuang, A. Telling, M. Hu, D. I. Martin, T. Enver, T. J. Ley, and M. Groudine. 1995. Targeted deletion of 5′HS2 of the murine beta-globin LCR reveals that it is not essential for proper regulation of the beta-globin locus. *Genes Dev.* 9: 2203–2213.
52. Hug, B. A., R. L. Wesselschmidt, S. Fiering, M. A. Bender, E. Epner, M. Groudine, and T. J. Ley. 1996. Analysis of mice containing a targeted deletion of beta-globin locus control region 5′ hypersensitive site 3. *Mol. Cell. Biol.* 16: 2906–2912.
53. Pham, C. T., D. M. MacIvor, B. A. Hug, J. W. Heusel, and T. J. Ley. 1996. Long-range disruption of gene expression by a selectable marker cassette. *Proc. Natl. Acad. Sci. USA* 93: 13090–13095.
54. Leder, A., C. Daugherty, B. Whitney, and P. Leder. 1997. Mouse ζ- and α-globin genes: embryonic survival, α-thalassemia, and genetic background effects. *Blood* 90: 1275–1282.
55. DeJarnette, J. B., C. L. Sommers, K. Huang, K. J. Woodside, R. Emmons, K. Katz, E. W. Shores, and P. E. Love. 1998. Specific requirement for CD3ε in T cell development. *Proc. Natl. Acad. Sci. USA* 95: 14909–14914.
56. Ren, S. Y., P. O. Angrand, and F. M. Rijli. 2002. Targeted insertion results in a rhombomere 2-specific Hoxa2 knockdown and ectopic activation of Hoxa1 expression. *Dev. Dyn.* 225: 305–315.
57. Scarff, K. L., K. S. Ung, J. Sun, and P. I. Bird. 2003. A retained selection cassette increases reporter gene expression without affecting tissue distribution in SPI3 knockout/GFP knock-in mice. *Genesis* 36: 149–157.
58. Hedger M. P., and D. B. Hales. 2005. Immunophysiology of the male reproductive tract. In *Knobil and Neill's Physiology of Reproduction*, 3rd Ed. J. Neill and P. Wassarman, eds. Academic, San Diego, pp. 1195–1250.
59. Geissler, W. M., D. L. Davis, L. Wu, K. D. Bradshaw, S. Patel, B. B. Mendonca, K. O. Elliston, J. D. Wilson, D. W. Russell, and S. Andersson. 1994. Male pseudohermaphroditism caused by mutations of testicular 17β-hydroxysteroid dehydrogenase 3. *Nat Genet* 7: 34–39.
60. Andersson, S., D. M. Berman, E. P. Jenkins, and D. W. Russell. 1991. Deletion of steroid 5α-reductase 2 gene in male pseudohermaphroditism. *Nature* 354: 159–161.
61. Schaller, C. E., C. L. Wang, G. Beck-Engeser, L. Goss, H. S. Scott, M. S. Anderson, and M. Wabl. 2008. Expression of Aire and the early wave of apoptosis in spermatogenesis. *J. Immunol.* 180: 1338–1343.
62. Schalkwyk, L. C., C. Fernandes, M. W. Nash, K. Kurrikoff, E. Vasar, and S. Koks. 2007. Interpretation of knockout experiments: the congenic footprint. *Genes Brain Behav.* 6: 299–303.
63. Yang, S., M. Farias, D. Kapfhamer, J. Tobias, G. Grant, T. Abel, and M. Bucan. 2007. Biochemical, molecular and behavioral phenotypes of Rab3A mutations in the mouse. *Genes Brain Behav.* 6: 77–96.
64. Gray, D., J. Abramson, C. Benoist, and D. Mathis. 2007. Proliferative arrest and rapid turnover of thymic epithelial cells expressing Aire. *J. Exp. Med.* 204: 2521–2528.
65. Taubert, R., J. Schwendemann, and B. Kyewski. 2007. Highly variable expression of tissue-restricted self-antigens in human thymus: implications for self-tolerance and autoimmunity. *Eur. J. Immunol.* 37: 838–848.
66. Sabater, L., X. Ferrer-Francesch, M. Sospedra, P. Caro, M. Juan, and R. Pujol-Borrell. 2005. Insulin alleles and autoimmune regulator (AIRE) gene expression both influence insulin expression in the thymus. *J. Autoimmun.* 25: 312–318.
67. Edwards, J. R., and T. H. Bestor. 2007. Gene regulation: stochastic and deterministic effects in gene regulation. *Heredity* 99: 243–244.
68. Hässler, S., C. Ramsey, M. C. Karlsson, D. Larsson, B. Herrmann, B. Rozell, M. Backheden, L. Peltonen, O. Kämpe, and O. Winqvist. 2007. Aire-deficient mice develop irregularities and marginal zone B-cell lymphoma. *Blood* 108: 1941–1948.
69. Li, J., Y. Li, J. Y. Yao, R. Jin, M. Z. Zhu, X. P. Qian, J. Zhang, Y. X. Fu, L. Wu, Y. Zhang, and W. F. Chen. 2007. Developmental pathway of $CD4^{+/-}CD8^-$ medullary thymocytes during mouse ontogeny and its defect in $Aire^{-/-}$ mice. *Proc. Natl. Acad. Sci. USA* 104: 18175–18180.